AD-A037 217 UNIVERSAL ENERGY SYSTEMS INC DAYTON OHIO F/G 20/9
ANALYSIS OF COMBUSTION PLASMAS BY FOURIER SPECTROSCOPY.(U)
DEC 76 C A DEJOSEPH, M LAKE F44620-76-C-0102
UNCLASSIFIED AFOSR-TR-77-0131 NL

1 OF 1
AD A037217

END

DATE FILMED
4-77

(13)
NW

UES
Universal Energy
Systems, Inc.

UNCLASSIFIED
SECURITY CLASSIFICATION OF THIS PAGE (When Data Entered)

REPORT DOCUMENTATION PAGE

READ INSTRUCTIONS BEFORE COMPLETING FORM

1. REPORT NUMBER: AFOSR - TR - 77 - 0131	2. GOVT ACCESSION NO.
3. RECIPIENT'S CATALOG NUMBER	
4. TITLE (and Subtitle): ANALYSIS OF COMBUSTION PLASMAS BY FOURIER SPECTROSCOPY.	5. TYPE OF REPORT & PERIOD COVERED: Final Report, 01 June 1976 - 30 September 1976
6. PERFORMING ORG. REPORT NUMBER	
7. AUTHOR(s): Charles A. DeJoseph, Jr. Max Lake	8. CONTRACT OR GRANT NUMBER(s): F44620-76-C-0102 new
9. PERFORMING ORGANIZATION NAME AND ADDRESS: Universal Energy Systems, Inc. 3195 Plainfield Road Dayton, OH 45432	10. PROGRAM ELEMENT, PROJECT, TASK AREA & WORK UNIT NUMBERS: 9751-02 61102F 92
11. CONTROLLING OFFICE NAME AND ADDRESS: AFOSR/NP Bolling AFB, DC 20332	12. REPORT DATE: 15 December 1976 13. NUMBER OF PAGES: 84
14. MONITORING AGENCY NAME & ADDRESS (if different from Controlling Office): 87p.	15. SECURITY CLASS. (of this report): UNCLASSIFIED 15a. DECLASSIFICATION/DOWNGRADING SCHEDULE

16. DISTRIBUTION STATEMENT (of this Report)

Approved for public release; distribution unlimited.

17. DISTRIBUTION STATEMENT (of the abstract entered in Block 20, if different from Report)

18. SUPPLEMENTARY NOTES

TECH, OTHER

19. KEY WORDS (Continue on reverse side if necessary and identify by block number)

Fourier Spectroscopy
Infrared Emission Spectroscopy
Combustion Analysis
Combustion Plasma
Combustion
Infrared Spectroscopy

20. ABSTRACT (Continue on reverse side if necessary and identify by block number)

Fourier Transform Spectroscopy has been used to study the infrared emission from a premixed, methane - air flame using a flat flame burner, in the region 1700 cm^{-1} to 7000 cm^{-1}. Some preliminary data was also obtained in the region from 400 cm^{-1} to 1700 cm^{-1}. All spectra were taken with 1 cm^{-1} resolution or better. Spectra were obtained at various heights above the burner base and under a variety of mix ratios. From the rotational structure in the CO fundamental band, rotational and vibrational temperatures were obtained for a rich fuel mix.

DD FORM 1 JAN 73 1473 EDITION OF 1 NOV 65 IS OBSOLETE

UNCLASSIFIED
SECURITY CLASSIFICATION OF THIS PAGE (When Data Entered)

390 743

(12)

ANALYSIS OF COMBUSTION PLASMAS

BY FOURIER SPECTROSCOPY

UNIVERSAL ENERGY SYSTEMS, INC.
3195 PLAINFIELD ROAD
DAYTON, OHIO 45432

SEPTEMBER 1976

FINAL REPORT FOR PERIOD 01 JUNE 1976 - 30 SEPTEMBER 1976

Approved for public release; distribution unlimited.

Prepared for

AIR FORCE OFFICE OF SCIENTIFIC RESEARCH
BUILDING 410
BOLLING, AFB, D. C. 20332

F44620-76-C-0102

TABLE OF CONTENTS

LIST OF ILLUSTRATIONS AND TABLES

ABSTRACT

Fourier Transform Spectroscopy has been used to study the infrared emission from a premixed, methane - air flame using a flat flame burner, in the region 1700cm^{-1} to 7000cm^{-1}. Some preliminary data was also obtained in the region from 400cm^{-1} to 1700cm^{-1}. All spectra were taken with 1cm^{-1} resolution or better. Spectra were obtained at various heights above the burner base and under a variety of mix ratios. From the rotational structure in the CO fundamental band, rotational and vibrational temperatures were obtained for a rich fuel mix.

ANALYSIS OF COMBUSTION PLASMAS BY FOURIER SPECTROSCOPY

I. Combustion Analysis

A. Objective

The purpose of this research is to establish the feasibility of using Fourier Transform Spectroscopy to analyze combustor plasmas of AF interest. The need to advance the quantitative knowledge of combustion processes stems from a combination of reasons. There exists a finite and exhaustible supply of conventional fossil fuel, dictating the requirements to maximize the efficiency of converting this fuel, as well as to develop alternate fossil fuels such as derivatives of shale oil and coal. Coupled with these requirements are existing and projected Federal regulations regarding exhaust emission in the troposphere and stratosphere.

B. Background

Theoretical modeling of the combustion plasma relies on a knowledge of the species in the plasma and their respective reaction rates. Basic data of this nature is still inadequate however. Tools for combustion diagnostics include probes, such as mass spectrometers, and several optical techniques. Mass spectrometer measurements yield data on the identity of the species and their relative concentration, but the technique is limited by its ability to sample only reaction products downstream from the source,

and by the fact that a variety of hydrocarbons have the same mass number. Two powerful optical techniques have recently been developed, but similarly do not yield a complete description of the physics of combustion. The laser raman scattering (LARS) signal from the combustion chamber is used to obtain spatially resolved profiles of the major species and temperature of the combustion plasma. This technique has limitations due to a lack of signal strength. Coherent antistokes Raman spectroscopy (CARS) offers a significant advantage over incoherent Raman spectrosocpy at atmospheric pressures in that the signal strength are several orders of magnitude larger than spontaneous Raman scattering for the same target density. While both the CARS and LARS requirements for high peak power tunable laser have been met in part by advances with tunable dye lasers, the applications are still limited to cooperative situations.

The emission and absorption of radiation associated with the combustion plasma contain detailed information about the combustion species and their reactions. Since the frequency of the radiation emitted or absorbed by a molecular gas is dependent on the energy level spacing of the molecule, and the relative intensities of the radiation is a function of the energy level population distribution,

the identity of the emitting or absorbing gas and its temperature can be obtained from analysis of the emission or absorption spectrum. The intensity of radiation in the infrared portion of the spectrum resulting from vibrational and rotational transitions is very weak, however, so that emission and absorption analysis have been applied most successfully in a laboratory environment. Now, with the implementation of Fourier transform spectroscopy (FTS), the sensitivity of infrared spectrometers have been increased by up to 100 times the sensitivity of dispersive systems. The power of FTS is that it is much faster than dispersive systems, and this speed may be used to improve the signal-to-noise ratio by coherent addition of signal. In addition, recent technical developments with data handling systems have greately enhanced the capabilities of FTS, allowing for rapid signal averaging and conversion from time to frequency domain, as well as sophisticated manipulation of data stored in the system. FTS has been successfully applied to studies of infrared spectra of aqueous solutions, kinetics of chemical reactions, and infrared chemiluminescence. Applied to combustion processes the FTS system assembled here has the capability to identify transient and product species in the combustion plasma, as well as the relative

concentration and temperature of the species. This will be demonstrated in the results for rotational temperature of a flue flame burner.

II. Fourier Transform Spectroscopy

A. Introduction

Fourier Transform Spectroscopy (FTS) is a multiplex technique for measuring the infrared power spectrum of an emitting source. Multiplexing implies than many separate streams of information are simultaneously transmitted along a single channel, and in FTS, information about a large number of spectral elements is simultaneously gathered through a single detection channel.[1] In an ordinary spectrograph, information about many spectral elements is gathered simultaneously by the photographic emulsion; however, each emulsion grain acts as a detection channel. Thus the ordinary spectrograph is not a multiplex system, it is more properly a multichannel system. In multiplex spectroscopy the intensity of each spectral element of a broad spectrum is coded, energy from the entire spectrum detected, and then the spectrum decoded. The coding used in FTS is the orthogonal functions sine and cosine. Specifically, the intensity of each spectral element $\delta\sigma$ ($\delta\sigma$ in cm^{-1} is the resolution of the instrument) is sinusoidally modulated

at a frequency which is proportional to the wavenumber of the element.[2] An advantage to this approach lies in the fact that since information about the entire spectral region is gathered simultaneously, there is a savings in measurement time over a sequential measurement technique, such as a normal monochrometer. To see this, let the spectral region of interest extend from σ_1 to σ_2. Then the number fo spectral elements in the region is given by;

$$m = \frac{\sigma_2 - \sigma_1}{\delta\sigma}$$

and the time to sequentially measure the spectrum is mT, where T is the time devoted to the measurement of a single element. In the multiplex technique, the time required to measure the entire spectral region is just T. If the measurement is detector-noise limited (the detector is the chief course of noise) then the signal-to-noise ratio associated with the measurement of a single element goes as the square root of the measurement time for the element. If one requires that the total measurement times for the two techniques be equal, say T, then the time devoted to each element in the sequential technique is T/m, while the time devoted to each element in the multiplex technique is T. In the first case, the signal-to-noise ratio goes as $(T/m)^{1/2}$

while in the second case it goes as $(T)^{1/2}$. Thus for a fixed total measurement time, the multiplex technique results in a signal-to-noise improvement of $m^{1/2}$ over a sequential measurement technique. This reduced measurement time or signal-to-noise improvement is known as the multiplex of Fellgett advantage.[1,2,3,4]

B. Basic Equations

To realize the multiplex advantage, the spectral information from the source must be coded and detected. The device that accomplishes this in FTS is the Michelson Interferometer (or one of its variants). Figure II illustrates an interferometer and its collimating optics. Radiation incident on the beam splitter-compensator is amplitude divided into two parts. These disturbances travel to mirrors M_1 and M_2 and are recombined by the beam-splitter-compensator after traveling over two different paths X_1 and X_2. The resultant disturbance is then focused on the detector. One of the mirrors is movable so that the path difference, $X_2-X_1=X$, can be varied. Consider the intensity that reaches the detector at a fixed path difference. Before doing so, consider the source to have the following properties:

(1) It is stationary, i.e. ensemble averages are independent of the origin of time.

BASIC MICHELSON INTERFEROMETER

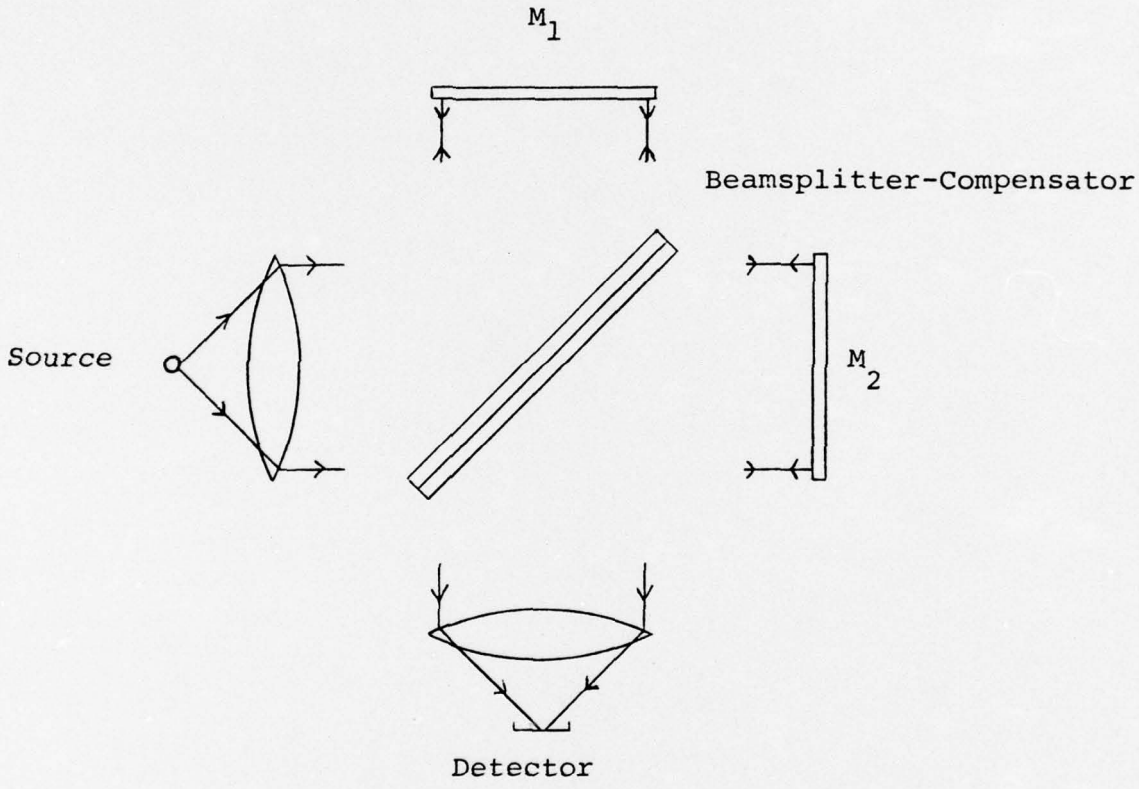

Figure II-1

(2) it is ergodic, i.e. ensenble averages are equal to the corresponding time averages of one of the representative members of the ensemble.

(3) The field vectors associated with the source possess fourier transforms.[5]

The real vector potential of the source at a point in space $\underline{S}$ (the bar under the symbol will designate a vector quantity) and time t is $\underline{A}(\underline{S},t)$. In the frequency domain the fourier transform of $\underline{A}(\underline{S},t)$ can be written:

$$\tilde{\underline{A}}(\underline{S},f) = \int_{-\infty}^{\infty} \underline{A}(\underline{S},t) e^{i2\pi ft} dt \qquad \text{II-1}$$

and from the theory of fourier integrals[6] one has:

$$\underline{A}(\underline{S},t) = \int_{-\infty}^{\infty} \underline{A}(\underline{S},f) e^{-i2\pi ft} df \qquad \text{II-2}$$

Equations II-1 and II-2 define a fourier transform pair $\underline{A}$ and $\tilde{\underline{A}}$. Next, denote the time average of a quantity y(t) as $\langle y \rangle$ and define $\langle y \rangle$ as:[5]

$$\langle y \rangle = \underset{T \to \infty}{\text{Limit}} \frac{1}{2T} \int_{-T}^{T} y(t) dt \qquad \text{II-3}$$

In most cases, y(t) is given by

$$y(t) = \begin{cases} y(t) & |t| \leq T_{max} \\ 0 & |t| > T_{max} \end{cases}$$

Then II-3 becomes

$$\langle y \rangle = \underset{T \to T_{max}}{\text{Limit}} \frac{1}{2T} \int_{-T}^{T} y(t)dt \qquad \text{II-3a}$$

The average intensity of the radiation at a point $\underline{S}$ is defined as

$$I(\underline{S}) = \left\langle |\underline{A}(\underline{S},t)|^2 \right\rangle. \qquad \text{II-4}$$

To find the intensity of the disturbance at the detector, consider the vector potential $\underline{A}$ incident on the beamsplitter-compensator. The vector potential is divided into two parts $\underline{A}_1$ and $\underline{A}_2$ that travel to mirrors M_1 and M_2. Each disturbance makes one reflection and one and one half passes through the beamsplitter-compensator before reaching the detector. Let the complex reflectance and transmittance of the beamsplitter-compensator be $r(f)$ and $\eta(f)$, and let the difference in time of arrival of the two disturbances, resulting from a difference in path, be τ. Then the magnitude of $\underline{A}_1$ and $\underline{A}_2$ are given by

$$A_1(\underline{S},t) = r\eta A(\underline{S},t)$$

$$A_2(\underline{S},t) = r\eta A(\underline{S},t+\tau)$$

The resultant amplitude at the detector is then

$$A_{res}(S_o,t) = r\eta A(S_o,t) + r\eta A(S_o,t+\tau) \qquad \text{II-5}$$

where S_o is the position of the detector, and the intensity at the detector, $I(S_o)$, is given by

$$I(S_o) = \left\langle |A_{res}(S_o,t)|^2 \right\rangle \qquad \text{II-6}$$

from equation II-4. Using equation II-5, and property (1) of the source, equation II-6 becomes

$$I(S_o) = 2|r\eta|^2 \cdot \left\{ \left\langle |A(S_o,t)|^2 \right\rangle + \left\langle A(S_o,t) \cdot A(S_o,t+\tau) \right\rangle \right\} \quad \text{II-7}$$

Since the source is collimated, one can write

$$\left\langle |A(S_o,t)|^2 \right\rangle = \left\langle |A(S,t)|^2 \right\rangle = I$$

where I denotes the intensity of the incoming radiation. Dropping the S_o, equation II-7 becomes

$$I(\text{Det}) = 2|r|^2 \cdot \left\{ I + \left\langle A(t) \cdot A(t+\tau) \right\rangle \right\} \quad \text{II-8}$$

Define[7]

$$\Gamma_{11}(\tau) = \left\langle A(t) \cdot A(t+\tau) \right\rangle$$

as the auto-correlation function of A(t), and define[7]

$$\gamma_{11}(\tau) = \Gamma_{11}(\tau)/I$$

as the normalized auto-correlation function of A(t). Then equation II-8 becomes:

$$I(\text{Detector}) \approx 2|r\eta|^2 \, I \cdot \left\{ 1 + \gamma_{11}(\tau) \right\} \quad \text{II-9}$$

for a time difference τ. Equation II-9 is a form of the basic equation used in FTS and expresses the intensity at the detector as a result of a disturbance with intensity I incident on the beamsplitter-compensator, and a time difference τ resulting from the radiation traveling a path difference X in the two arms of the interferometer. To express equation II-9 as a function of path difference and the power spectrum of the source, consider equation II-4.

Substituting the expression for $\underline{A}$ from equation II-2 into II-4 one finds:

$$I(S) = \underset{T\to\infty}{\text{Limit}} \frac{1}{2T}\int_{-T}^{T} |\underline{A}(\underline{S},t)|^2 dt$$

$$= \underset{T\to\infty}{\text{Limit}} \frac{1}{2T}\int_{-\infty}^{\infty} |\tilde{\underline{A}}(\underline{S},f)|^2 df \qquad \text{II-10}$$

which is essentially Parseval's theorem.[6] Define[5,7,8] the following

$$G(\underline{S},f) = \underset{T\to\infty}{\text{Limit}} \frac{|\tilde{A}(S,f)|^2}{2T} \qquad \text{II-11}$$

as the power spectrum in the frequency domain f. Since $\underline{A}(\underline{S},t)$ is real it can be shown[6] that equation II-10 can be written;

$$I(\underline{S}) = 2\int_{0}^{\infty} G(\underline{S},f)df \qquad \text{II-12}$$

and it can also be shown that the normalized auto-correlation function γ_{11} (dropping the spatial dependence) can be written[8]:

$$\gamma_{11}(\tau) = \frac{\int_{0}^{\infty} G(f)\cos 2\pi f\tau df}{\int_{0}^{\infty} G(f)df} \qquad \text{II-13}$$

Substituting II-12 and II-13 into II-9 gives (I)is the intensity at the detector

$$I(\tau) = 2|r\eta|^2 \cdot \int_0^\infty 2G(f)[1+\cos 2\pi f\tau]df. \qquad \text{II-14}$$

Finally, going from the frequency-time domains to wavenumber-length domains one makes the following substitutions:

$\tau = \frac{x}{c}$ $\qquad$ c = speed of light

$f = c\sigma$ $\qquad$ σ = wavenumber(cm^{-1})

and let $2cG(c\sigma) = B(\sigma)$ be the power spectrum in the wavenumber domain, then equation II-14 becomes

$$I(x) = 2|r\eta|^2 \int_0^\infty B(\sigma)[1+\cos 2\pi\sigma x]d\sigma \qquad \text{II-15}$$

Where x = path difference between the two mirrors

r = reflectance of the beamsplitter-compensator

η = transmittance of the beamsplitter-compensator

$B(\sigma)$ = power spectrum of the radiation in the wavenumber domain

I(x) = the intensity at the detector for a path difference x

Thus I(x) consists of a constant term plus a fluctuation

term. Let the fluctuating part of I(x) be dI(x) then equation II-15 becomes

$$dI(x) = 2|r\eta|^2 \cdot \int_0^\infty B(\sigma)\cos 2\pi\sigma x d\sigma. \qquad \text{II-16}$$

From the orthogonality properties of the cosine functions, equation II-16 can be solved for $B(\sigma)$ and one finds

$$B(\sigma) = \frac{2}{|r\eta|^2} \cdot \int_0^\infty dI(x)\cos 2\pi\sigma x dx \qquad \text{II-17}$$

Equations II-16 and II-17 are the basic equations of FTS. The quantity dI(x) is called the interferogram, and equation II-17 shows that the power spectrum of the source can be obtained from a fourier cosine transform of the interferogram. It is also clear from equation II-16 that the intensity at the detector, for a given path difference, contains information about the entire spectral region of $B(\sigma)$.

C. Recovery of the Spectrum

Implementation of the FTS technique requires the interferogram dI(x) to be recorded as a function of path difference x. In practice, x is continuously varied by moving one of the mirrors at velocity v while the fluctuating component of the signal from the detector is recorded. Two difficulties immediately arise in the actual measurement.

1) In general, equation II-17 must be solved by a digital computer so dI(x) must be digitized and recorded as a discreet set of points $dI(x_j)$ as opposed to an analytic function.

2) The limits on equation II-17 imply that one of the mirrors must be moved an infinite distance. Since this is not possible, the mirror is moved only over some finite distance L.

Consider the effects of these departures from the ideal theoretical equations II-16 and II-17. To arrive at the effect of finite mirror travel define the function

$$a(x) = \begin{cases} 1 & x \leq \chi \\ 0 & x > \chi \end{cases}$$

where χ is the maximum path difference attainable. Equation II-17 can be written

$$B_r(\sigma) = \frac{2}{|r\eta|^2} \int_{-\infty}^{\infty} a(x)\,dI(x)\cos 2\pi\sigma x\,dx$$

where $B_r(\sigma)$ denotes the recovered spectrum under the conditions of finite path difference. Taking the fourier transform of $B_r(\sigma)$ one has

$$FT[B_r(\sigma)] = a(x)\,dI(x)$$

and for the ideal spectrum

$$FT[B(\sigma)] = dI(x)$$

Then writing a(x) as:

$$a(x) = FT[\tilde{a}(\sigma)]$$

one has:

$$FT[B_r(\sigma)] = FT[B(\sigma)] \cdot FT[\tilde{a}(\sigma)].$$

Using the convolution theorem[6] one has from the above;

$$B_r(\sigma) = B(\sigma) * \tilde{a}(\sigma) \qquad \text{II-18}$$

where $B(\sigma) * \tilde{a}(\sigma)$ is the convolution of $B(\sigma)$ and $\tilde{a}(\sigma)$ and is defined as[6]

$$B(\sigma) * \tilde{a}(\sigma) = \int_{-\infty}^{\infty} B(u)\tilde{a}(\sigma-u)du. \qquad \text{II-19}$$

To see the effect of the convolution of B and a consider the expression for $\tilde{a}(\sigma)$;

$$\tilde{a}(\sigma) = \int_{o}^{\chi} \cos 2\pi x\sigma dx = \frac{\sin 2\pi\sigma\chi}{2\pi\sigma}$$

Thus one sees that the recovered spectrum B_r is a smeared out version of B due to the convolution of B with the sinc function.[2] The Rayliegh criterion for resolving two spectral features is that the peak of one feature falls at the first zero of the second feature. The first zero of the sinc function occurs at $2\pi\sigma\chi = \pi$, so using the Rayliegh criterion, the resolution $\delta\sigma$ is given by:

$$2\pi\delta\sigma\chi = \pi$$

or

$$\delta\sigma = \frac{1}{2\chi} \qquad \text{II-21}$$

Thus the effect of finite mirror travel is to determine the resolution of the instrument.

The effects on the recovered spectrum due to the discreet nature of the sampled interferogram range from signal-to-noise degradation[9] to determining the spectral bandwidth that can be recovered from the sampled interferogram.[2,3,4] It is this latter effect that must be carefully controlled in order to avoid recovering a false spectrum. The results of sampling the interferogram will not be derived but will be stated. The sampling theorem[2,3,4] states that one must sample the data at a rate equal to the reciprocal of twice the highest frequency present in the data in order to avoid overlapping or aliasing. In equation II-16, for a given displacement, the highest frequency present is σ_{max}, where σ_{max} is the highest wavenumber present in the spectrum $B(\sigma)$. Therefore if Δx is the sample spacing of the interferogram, the sampling theorem requires that:

$$\Delta x \leq \frac{1}{2\sigma_{max}} . \qquad \text{II-22}$$

That is, the sample spacing must be less than or equal to the reciprocal of twice the highest wavenumber present in the spectrum. If relation II-22 is not adhered to, the recovered spectrum $B_r(\sigma)$ will be aliased or folded back on itself and thus will not give an accurate measure of $B(\sigma)$. In practice, one usually uses a low pass spectral filter to insure that no wavenumber greater than σ_{max}

enters the interferometer for the sample spacing chosen. For example, if one desires to investigate the spectrum from a source in the wavenumber range 0 to 7000cm^{-1}, the interferogram dI(x) must be sampled every 7.1428 X 10^{-5}cm of path difference.

To recover the spectrum $B_r(\sigma)$ from the interferogram dI(x), the procedure is thus to record the interferogram dI(x) at path differences of x_j, where $x_j - x_{j-1} = \Delta x$ is given by relation II-22, over a path difference χ determined by the desired resolution as given in II-21 and then solve equation II-17, which for the discreet case becomes:

$$B_r(\sigma_n) = \frac{2}{|r\eta^2|} = x \sum_{m=0}^{\infty} dI(x_m)a(x_m)\cos 2\pi\sigma_n x_m \quad \text{II-23}$$

where

$$x_m = m\Delta x$$

and a (x_m) is the truncating function described earlier. There are other, more subtle steps that must be taken before $B_r(\sigma)$ can be realized, and indeed there are subtle difficulties associated with the solution of II-23 involving manipulating large data files and computing times, however the basic procedures for recovering the power spectrum have been outlined. The reader is refered to references 2,3, and 4 for detailed discussions of the FTS technique.

D. Advantages of FTS

In the introduction to this section the multiplex nature of FTS was shown to yield an advantage in either short measurement time or signal-to-noise over a sequential measurement technique such as an ordinary monochrometer. There are two other distinct advantages of FTS that we will briefly discuss at this time. As mentioned in the previous section, the sample spacing of the data points in the interferogram is important in determining the maximum spectral bandwidth that can be unambiguously recovered in FTS. From the example given, to do mid-infrared spectroscopy (400-4000cm^{-1}) the path difference (and position of the moving mirror) must be known very accurately. At first this might appear to be a great disadvantage, and indeed if the problem had not been solved it would be, but the solution yields an advantage in FTS over most other spectroscopic techniques. To solve the problem of knowing the path difference very accurately the interferograms produced by a very broad band source and a near monochromatic source are used as measuring tools. It is seen from equation II-16, by letting $B(\sigma)$ be given by:

$$B(\sigma) = \begin{cases} \text{constant}, & \sigma \leq \sigma_{max} \\ 0, & \sigma > \sigma_{max} \end{cases}$$

that the interferogram essentially becomes a sinc function and thus peaks sharply at $x=0$. The broader the spectrum, the narrower the peak. In this way, a very broad-band source can give a good indication of zero path difference for the interferometer. Similarly, a near monochromatic source yields an interferogram that is essentially a cosine function of $2\pi\sigma_o x$, where σ_o is the wavenumber of the source. Thus, a near monochromatic source yields a waveform that can be used to measure x, provided σ_o is known. The interferometer used in this work actually consists of three interferometers to utilize the interferograms just discussed. Figure II-2 shows the configuration for this system of interferometers. The "white light" source is a broad-band incandescant bulb that is used as a reference point for zero path difference, and the HeNe laser is a near monochromatic source that supplies a cosine wave by which the path difference can be very accurately measured. This arrangement yields an absolute vacuum wavenumber determination to $.01 cm^{-1}$. Normally, one would be required to use infrared standards and correct for wavenumber in air to achieve this kind of accuracy; however, with the FTS system, the accuracy is automatically achieved.[4] This advantage is sometimes called Connes' advantage.

Another advantage of FTS is in its' high throughput

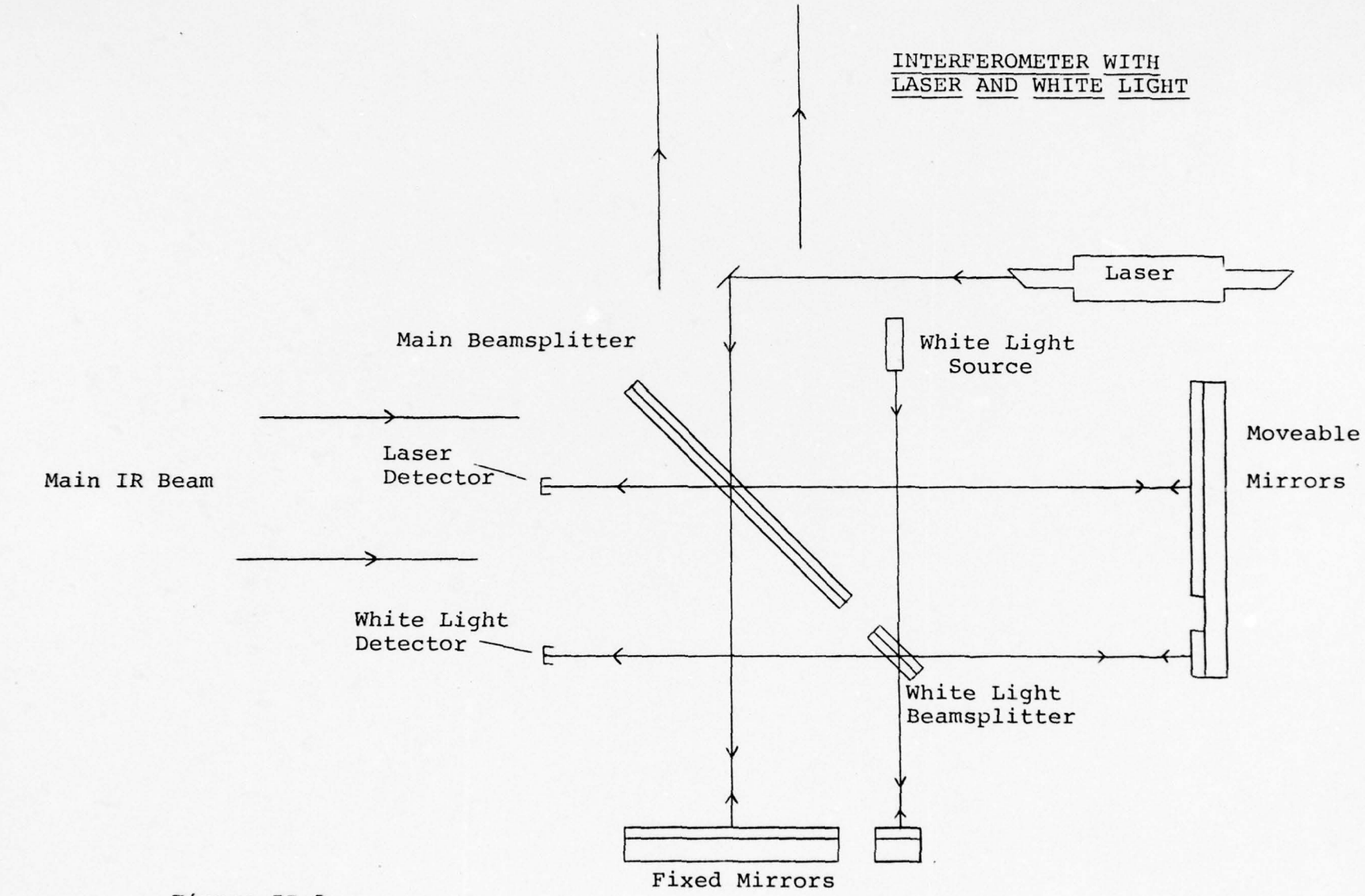
INTERFEROMETER WITH
LASER AND WHITE LIGHT
Laser
Main Beamsplitter
White Light
Source
Moveable
Mirrors
Laser
Detector
Main IR Beam
White Light
Detector
White Light
Beamsplitter
Fixed Mirrors

Figure II-2

or étendue. The energy available at the detector is given by:

$$I(\sigma) = T\, B(\sigma)\, E \qquad \text{II-24}$$

where T is the transmission of the system, $B(\sigma)$ is the intensity of the source at wavenumber σ, and E is the throughput of the system defined as;

$$E = A\Omega \qquad \text{II-25}$$

where A is the usable cross sectional area of the collimated beam and Ω is the solid angle subtended by the detector collection optics. It can be shown[2,3,4] that the maximum allowable detector solid angle is governed by the desired resolution and is given by

$$\Omega = \frac{2\pi}{R} \qquad \text{II-26}$$

where R is the resolving power $\sigma/\delta\sigma$. Using Equation II-26, equation II-24 can be written

$$I = \frac{TB2\pi A}{R}$$

or

$$IR = 2\pi TBA \qquad \text{II-27}$$

From II-27 one can see that there is a trade-off between resolving power and intensity at the detector; however, the product IR does not vary. For a conventional spectrometer the solid angle Ω is given by[2]

$$\Omega = \frac{wl}{f^2} \qquad \text{II-28}$$

where l is the slit height, w is the slit width and f is the focal length of the collimator. If the spectrometer has a dispersion $d\theta/d\sigma$ the resolution is given by

$$\delta\sigma = \frac{w}{f} \frac{d\theta}{d\sigma}$$

thus the resolving power is given by

$$\frac{\sigma}{\delta\sigma} = R = \frac{d\theta}{D\sigma} f \frac{\sigma}{w}$$

so that the slit width is

$$w = \frac{d\theta}{d\sigma} f \frac{\sigma}{R} . \qquad \text{II-29}$$

From II-24, II-25, II-28, and II-29 the product IR for the conventional spectrometer becomes

$$IR(conv) = TBA \frac{d\theta}{d\sigma} \sigma \frac{l}{f} . \qquad \text{II-30}$$

For a conventional spectrometer, a grating yields the highest value for the dispersion and in M^{th} order one has[5]

$$\sigma = \frac{m}{f} \csc \theta$$

so that

$$\left| \frac{d\theta}{d\sigma} \cdot \sigma \right| = \tan \theta$$

and for a grating angle of about 45° one has

$$\left| \frac{d\theta}{d\sigma} \cdot \sigma \right| \simeq 1$$

Then equation II-31 becomes

$$IR(conv) = TBA \frac{l}{f} .$$

For a conventional spectrometer the values (1/f) are very low compared to 2π and typically are of the order 1/50.[2] Thus FTS enjoys a throughput gain of the order of 50 over a conventional spectrometer. This advantage is usually called Jacquinot's advantage.

One other advantage of FTS is its relative insensitivity to stray light. Since each wavenumber σ is modulated at a different frequency, and only light nearly parallel to the moving mirror is modulated, FTS offers a vast improvement over a conventional spectrometer in insensitivity to stray light.[4] In summary, FTS offers at least four advantages over the conventional infrared spectrometer. They are:

1) Multiplex advantage (Fellgett advantage)
2) High wavenumber accuracy (Connes advantage)
3) High étendue or throughput (Jacquinot's advantage)
4) Stray light insensitivity

With fast detectors and high mirror velocities, FTS also has the advantage of very rapid data acquisition, which along with the above mentioned advantages, make it very suitable for mid-infrared emission studies.

III. Description of the Experiment

Figure III-1 shows the basic layout used to study the infrared emission from a small combustor. The major components in the experiment are A. the combustor, B. collection optics, C. interferometer-detector system, and D. data reduction system.

A. The Combustor

The combustor chosen for the study was a flat flame burner[10], so named for the appearance of the flame it produces. The flame has the characteristic that the interaction volume is large in comparison to the boundary layer, so that boundary layer effect can be ignored. The surface of the burner had a diameter of approximately 2.5 cm., and could be moved vertically by a precision screw-adjustment. The burner was housed in a water cooled, copper cylinder of approximately 7.5 cm. diameter, equipped with ports for observing the flame. The fuel used was low purity methane (commercial grade, approx. 90%) which was premixed with air before being burned. Normally, the ratio of air to methane was approximately 7:1 by volume, which yielded a very stable, flat flame that appeared to extend a few millimeters above the burner surface.

B. Collection Optics

A requirement for the interferometer is that the light source be collimated. The collimating lens used was a

LAYOUT OF EXPERIMENT

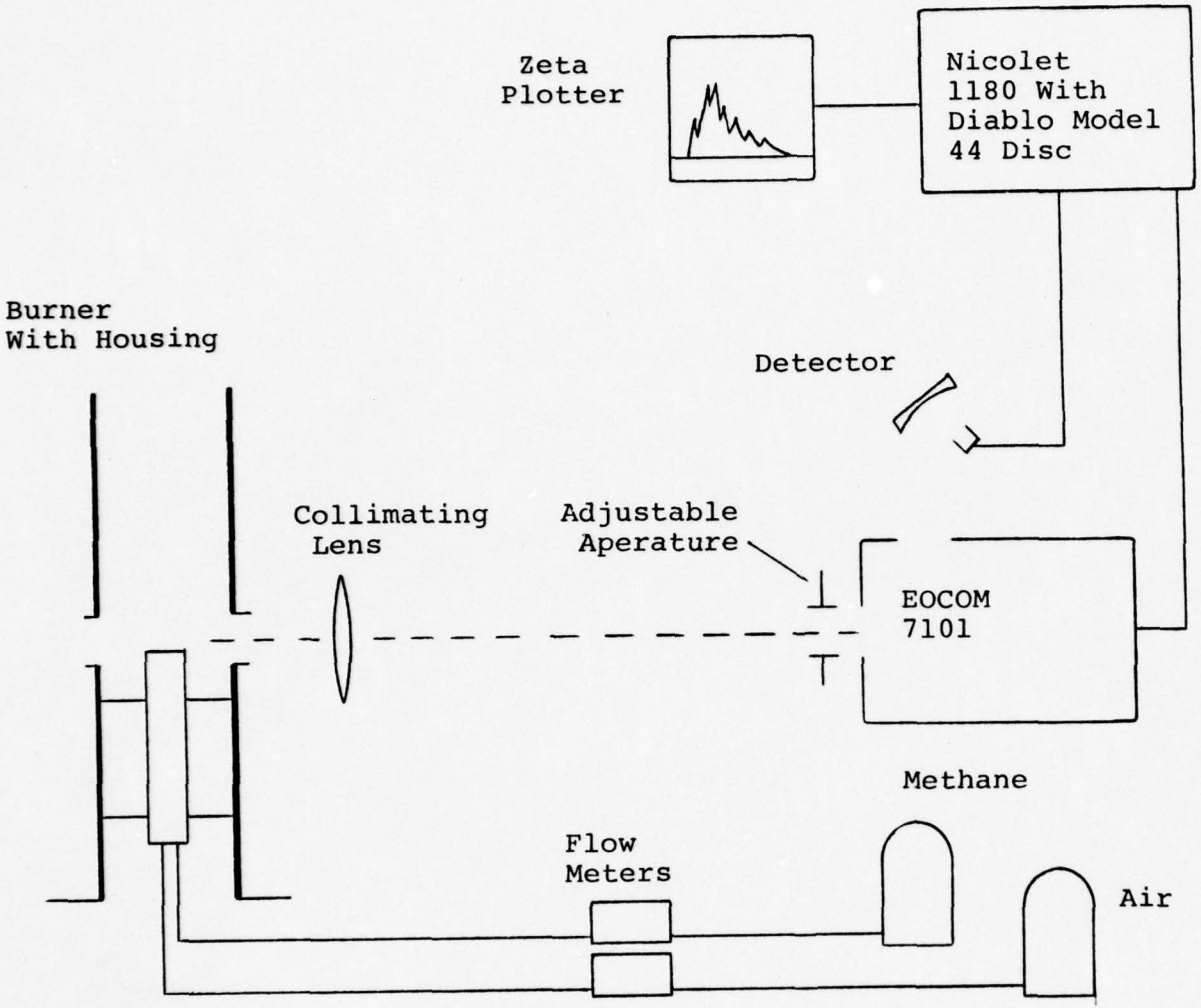

Figure III-1

100 mm. focal length, f/2 As_2S_3 - CaF_2 separated doublet with a useful transmission range from approximately 1250cm^{-1} to 12500cm^{-1} (8μm to .8μm). The lens was free of chromatic aberration between approximately 1800cm^{-1} and 2900cm^{-1} (5.5μm to 3.5μm), and had minimum chromatic aberration throughout its useful range. A 100mm focal length, f/2, NaCl lens was used briefly for measurements below 1250cm^{-1} (above 8μm). As shown in equation II-26, the resolving power of the interferometer is dependent on the solid angle subtended by the detector collection optics. Since the flame was in no way a point source, and it was impossible to place an aperture in the flame, it was necessary to limit the effective source size by some other means. This was achieved by placing approximately a 1cm aperture at the entrance to the interferometer, 45cm from the collimating lens. This alone, however, was not sufficient to achieve .06 cm^{-1} resolution, so an adjustment to the interferometer was necessary which will be discussed in the next part of this section of the report.

C. The Interferometer-Detector System

The interferometer used was essentially an EOCOM model FMS 7101 with the magnetic tape system disconnected. The instrument has greater than .06cm^{-1} resolution capability over the wavenumber range 400cm^{-1} to 7000cm^{-1} and is capable

of mirror velocities up to 4cm/sec. Thus, rapid scanning of a broad spectral retion is possible, with all of the advantages of the FTS technique discussed in section III. The beamsplitter-compensator normally used was Fe_2O_3 coated CaF_2 with a spectral range from 1250cm^{-1} to about 7000cm^{-1} (8μm to 1.4μm); however, a Ge coated KBr beamsplitter-compensator was briefly used for measurements below 1250cm^{-1} (above 8μm). Two detectors were used during the course of the investigation. Initially, a pyroelectric detector (triglycine sulfate, TGS) was used with the CaF_2 beamsplitter; however, the TGS detector's poor detectivity ($D^* \simeq 6X10^8$cm $Hz^{.5}$/watt) and slow time constant made spatially resolved measurements practically impossible. Late in the investigation, a thermoelectrically cooled PbSe detector was made available with a much higher detectivity ($D^* \simeq 2X10^{10}$), a much faster time constant, but with a somewhat more limited useful spectral range. This allowed spatially resolved data to be acquired in the wavenumber range 1700cm^{-1} to 7000cm^{-1} (5.9μm to 1.4μm). The final beamsplitter-detector combinations chosen were the CaF_2 - PbSe for the region 1700cm^{-1} to 7000cm^{-1} and the KBr - TGS for the region from 400cm^{-1} to 1700cm^{-1}. Very little data was taken in the latter region due to the poor performance of the TGS detector. The detectors were placed 30° off axis at the focal point of a 5cm diameter, 10 cm focal length parabola, to effectively increase their collection area.

As mentioned in part B, it was necessary to further reduce the solid angle subtended by the collection optics from the limit set by the aperture placed at the interferometer entrance. To achieve .06cm^{-1} resolution at 7000cm^{-1} the solid angle must be less than $5.39X10^{-5}$ sterradians, which corresponds to an angle of deviation for rays entering the interferometer of less than .237° or 4.14 mrad. This was difficult to achieve without sacrificing a large portion of signal, and in view of the fact that most of the emission from the flame occurred in the vicinity of 2000cm^{-1}, a compromise was reached. The solid angle was limited to about 1.8×10^{-4} sterradians, which was adequate to yield better than .06cm^{-1} resolution, and line position accuracy to better than .03cm^{-1} at 2000cm^{-1}. This was achieved by limiting the effective collection area of the detectors from the $\approx$20cm^2 of the parabola to about 0.2cm^2. This limiting of off-axis rays from entering the interferometer and being detected resulted in spatial resolution in the flame of approximately 1.5mm perpendicular to the optical axis.

D. Data Reduction System

The data reduction system consisted of a Nicolet 1180 signal averager/data processor with a CRT display for visual inspection and manipulation of data and a Zeta model 160 digital plotter for producing hard copy data plots. In addition, a Diablo model 44 dual disk random access storage

device was used for storing data and machine code instructions. The system was used in two basic modes. For moderate to low resolution($\delta\sigma \geq 1cm^{-1}$), data was acquired into the 1180, processed (fourier transformed), and the resulting spectrum stored on disk. This mode allowed data points to be taken at a rate of 50KHz, so that a $1cm^{-1}$ resolution interferogram (16384 data points) could be acquired in approximately 0.33 sec. and could be transformed in another 22 sec. (32K transform points). Low resolution, $4cm^{-1}$ scans could be taken in less than 0.09 sec. and could be transformed in 5 sec. It was therefore possible to obtain a spectrum of the burner over the region $1700cm^{-1}$ to $7000cm^{-1}$ (5.9μm to 1.4μm) with $4cm^{-1}$ resolution is 5 sec. The second mode of data collection was necessary for higher resolution spectra and consisted of acquiring data directly onto disk, processed, and the resulting spectrum stored back on disk. This mode dictated a somewhat slower data collection rate of 20KHz, so that a $.5cm^{-1}$ resolution scan (32768 data points) could be acquired in 1.64 sec. and could be transformed (64K transform points) in about 3 minutes. A $.06cm^{-1}$ scan (262000 data points) required 13 sec. to complete, and required about 28 minutes to process (524K transform points). In comparison, the time required to duplicate the $.06cm^{-1}$ resolution scan of the same spectral region with a conventional monochrometer (with the

same signal to noise ratio) would have required 322 hours (assuming the throughput of the two spectrometers is the same) and would still not yield the stray light advantage, or Connes' advantage (see section II). An important feature of the 1180 data reduction system was its capability for co-adding scans from the interferometer. In this way, the signal to noise ratio of the final spectrum could be improved by as much as a factor 5000 over the signal to noise ratio of a single scan. This, of course, required longer measurement times so usually some compromise was reached concerning acceptable signal to noise requirements. The data reduction system also allowed for data file manipulation (subtracting spectra, wavenumber to wavelength conversion, scaling, etc.) which greatly enhanced the capabilities of the interferometer.

IV. Results

Emission spectra were obtained of the flat flame burner, using a pre-mixed CH_4-air mixture, in the spectral region $1700cm^{-1}$ to $7000cm^{-1}$ (5.9μm to 1.4μm) with approximately a 1.5 meter air path between burner and detector. Spectra were obtained under a variety of experimental conditions including variation of the fuel-air mix ratio, moderate and high resolution, and collecting data from different regions of the flame. Some preliminary results were also obtained in the spectral region from $400cm^{-1}$ to $1700cm^{-1}$ (25μm to 5.9μm); however, data was only obtained under one set of the aforementioned conditions. Only relative intensities were obtained, therefore only a wavenumber scale appears on the data plots, the vertical scale being arbitrary units. The data was not corrected for the spectral response of the system, due to the late acquisition of the PbSe detector; however, a brief discussion of the general behavior of the system function will be given later. The data plots will be referred to in the text by figure number, i.e. figure IV-1, however, many of the plots occupy more than one report page so these figures will be labeled IV-1.1, IV-1.2, etc. to indicate multi-page figures.

A. Survey Spectra - Since the flame was observed through air, it was necessary to realize the effects of infrared absorption by the atmosphere in the spectral range of interest.

FIGURE IV-1.1

GLOWBAR SPECTRUM-1.5 METER AIR PATH
RESOLUTION= 1CM^{-1}
NUMBER OF SCANS= 256

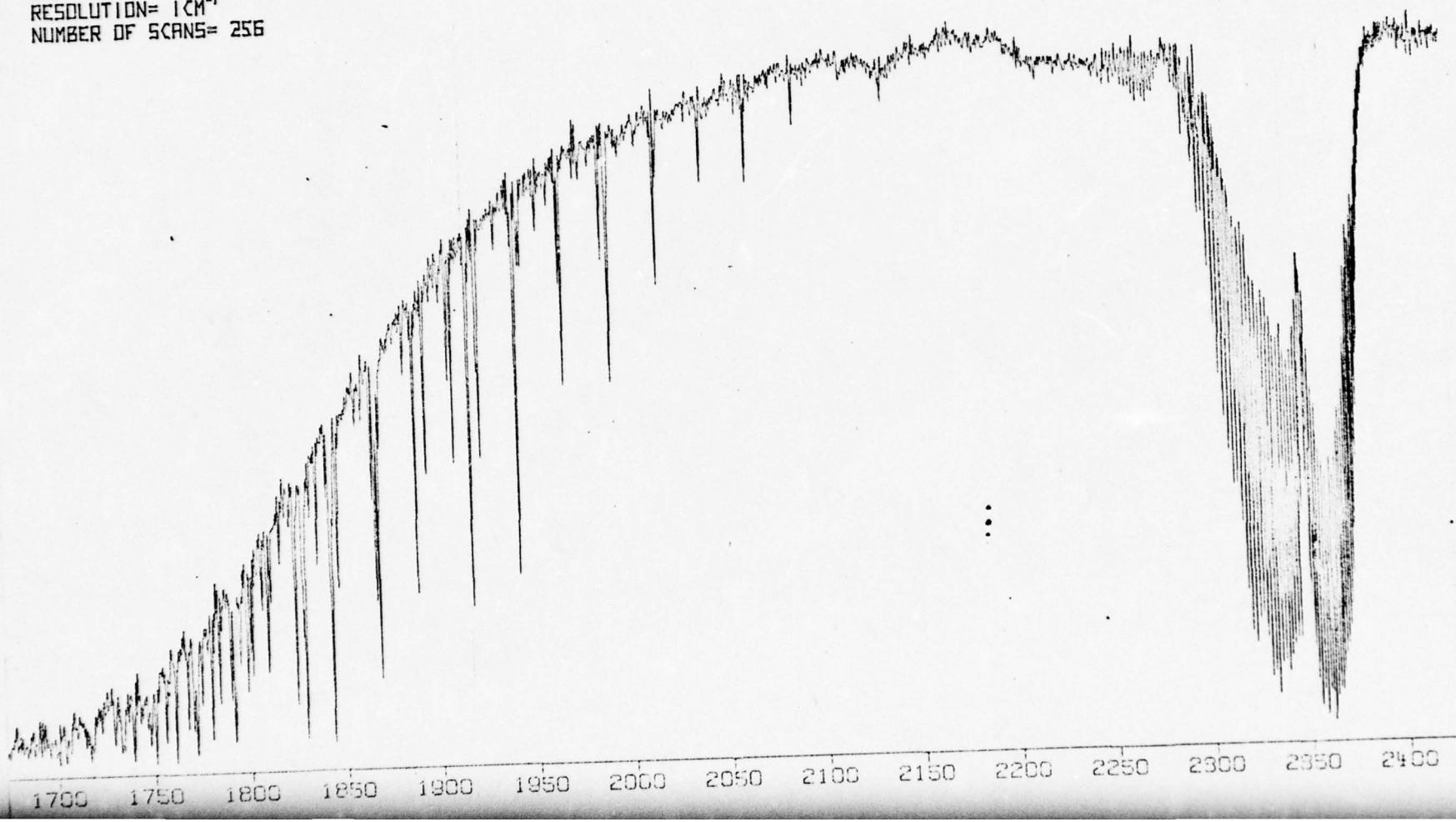

FIGURE IV-1.2

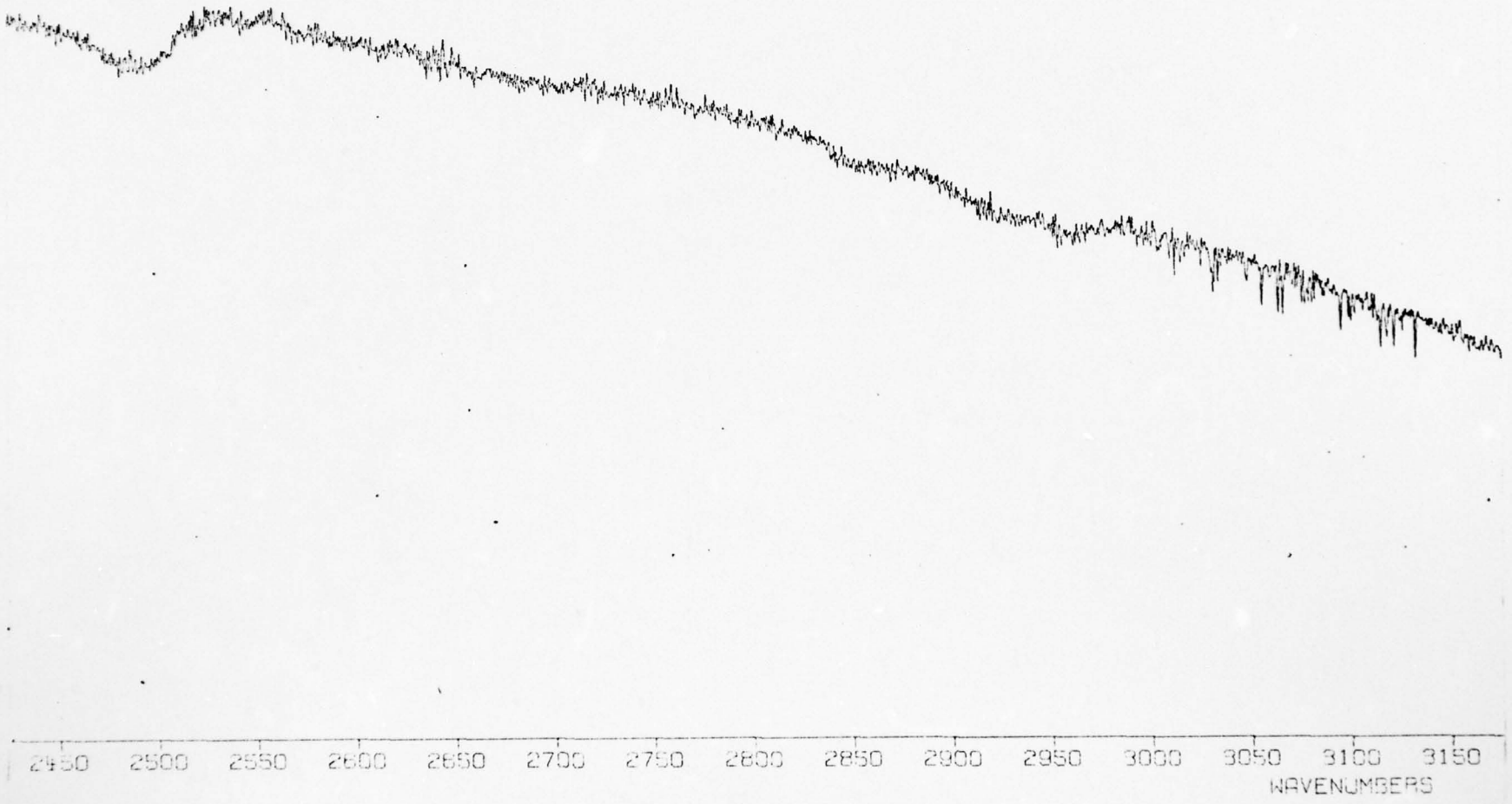
2450
2500
2550
2600
2650
2700
2750
2800
2850
2900
2950
3000
3050
3100
3150
WAVENUMBERS

FIGURE IV-1.3

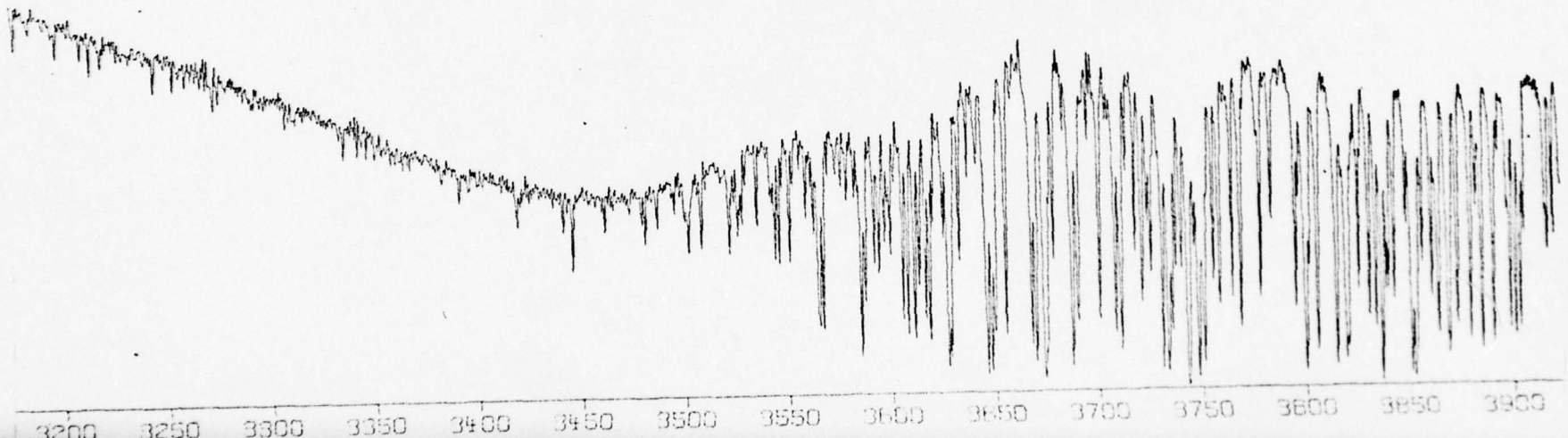
3200
3250
3300
3350
3400
3450
3500
3550
3600
3650
3700
3750
3800
3850
3900

0550
0554
0558
0562
0566
0570
0574
0578
0582
0586
0590
0594
0598
0602
0606
0610
0614
0618
0622
0626

FIGURE IV-1.4

FIGURE IV-1.5

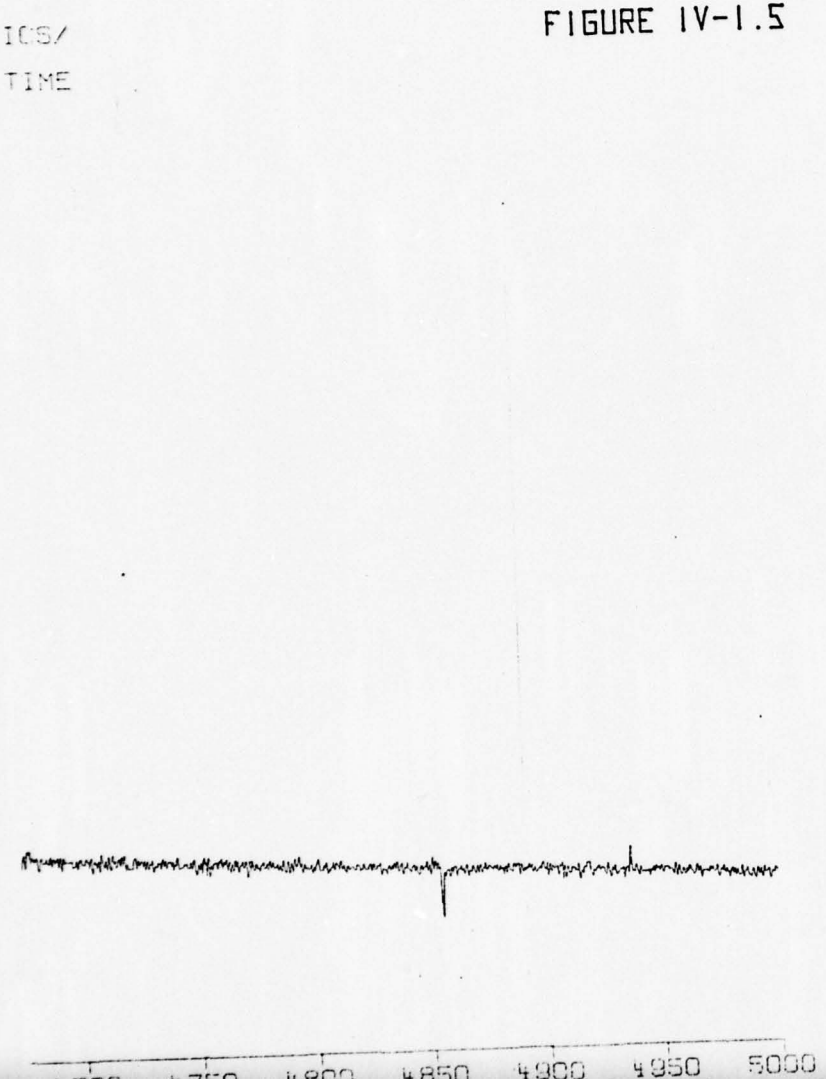

Figure IV-1 is the spectrum of a 1500°K "glowbar" measured through 1.5 meters of air with approximately $1cm^{-1}$ resolution. Data was collected up to $7000cm^{-1}$; however, no absorption was observed above $5000cm^{-1}$ so the plot was terminated at this point. The glowbar spectrum is roughly that of a black-body radiator, therefore it produces a continuous spectrum that can be approximated by the Planck equation.[10] The collection optics, detector, and beamsplitter were as discussed in section III. The number of scans on the plot indicates the number of single scan interferograms that were co-added before being processed. It can be seen that there is strong absorption in three regions of the spectrum; a) water vapor absorption in the vicinity of $1700cm^{-1}$ (6.3μm band), b) CO_2 absorption in the vicinity of $2350cm^{-1}$ (4.3μm band), and c) water vapor absorption (2.7μm band) and CO_2 absorption (2.7μm band) in the vicinity of $3700cm^{-1}$.[11] There is also some weak absorption in the vicinity of $3100cm^{-1}$ which is also due to water vapor.[11] By comparing figure IV-1 with a theoretical black-body function, the approximate behavior of the system response function can be obtained. The response function obtained in this manner is approximate because, a) the glowbar does not yield a true black-body spectrum, and b) the presence of atmospheric absorbers distorts the measured spectrum. The general

behavior of the system response function, however, can be obtained in this manner. Figure IV-2 shows the results of this calculation. The curve was obtained by dividing points on the measured plot by the predicted irradiance from a black-body, normalizing the data to the maximum value, and interpolating the data with a cubic spline. The sharp drop in sensitivity below $1950cm^{-1}$ is due to the cutoff of the PbSe detector and the broad dip in the curve between $2600cm^{-1}$ and $3000cm^{-1}$ is due to the transmission characteristics of the As_2S_3 lens component. The gradual decrease in sensitivity above $2200cm^{-1}$ is also primarily the result of the decreased responsivity of the PbSe detector.

Figure IV-3 is the spectrum obtained of the flat flame burner with approximately 0.25 cm^{-1} resolution. As in figure IV-1, data was obtained from $1700cm^{-1}$ to $7000cm^{-1}$; however, no interesting features were observed above $5000cm^{-1}$ so the plot was terminated at this point. The data was collected from a region of the flame approximately 10mm above the burner base. The actual shape of the region over which data was collected is difficult to calculate precisely; however, from simple ray tracing one finds that the volume sampled is roughly a cone 11mm high and 1.5mm at the base, oriented along the optical axis of the system. Since the flame is very uniform along the optical axis, the important parameter is the height above the burner base the data was taken. The strongest features in the spectrum are a) predominantly H_2O emission between $1700cm^{-1}$ and $2050cm^{-1}$,

FIGURE IV-2

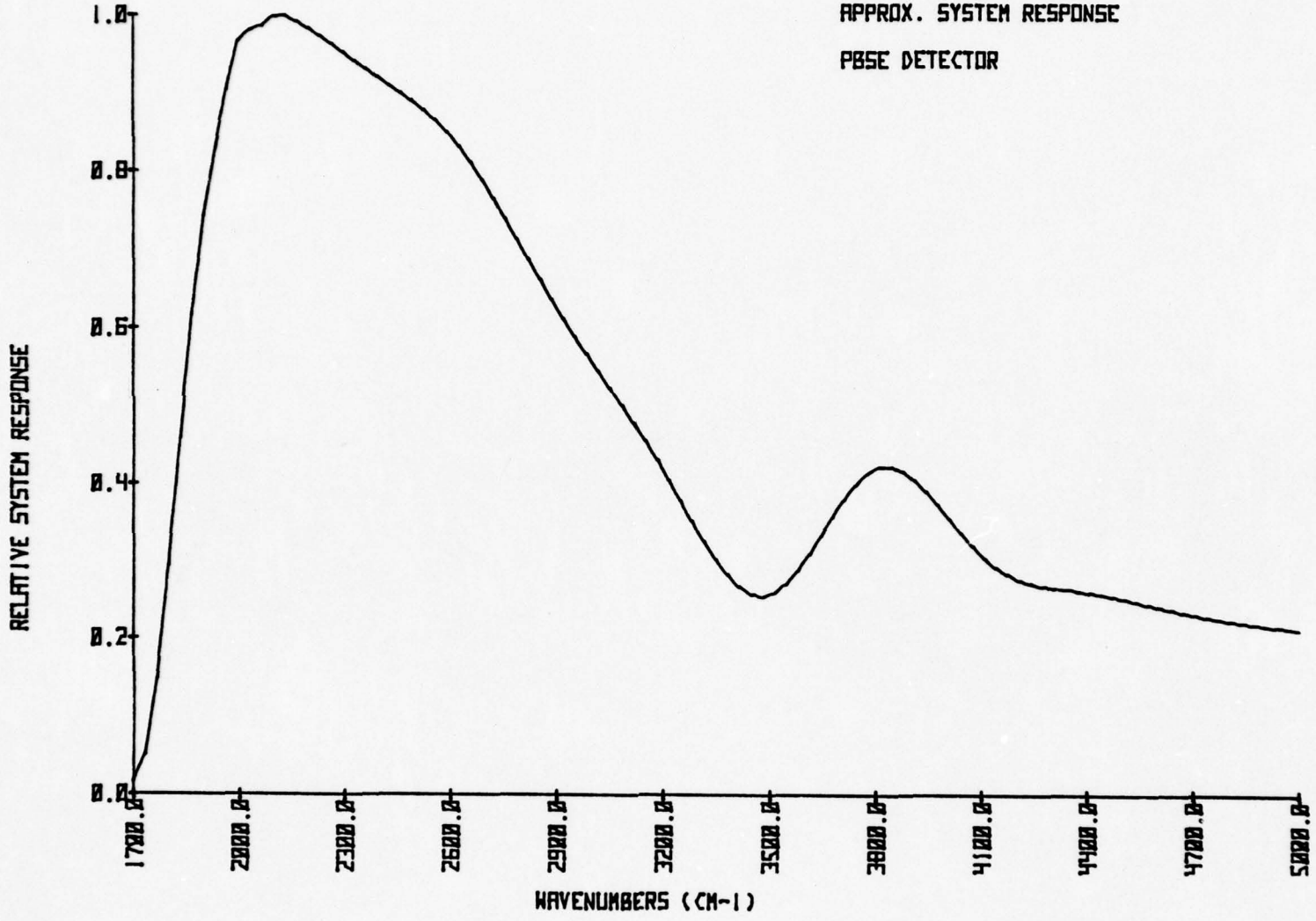
APPROX. SYSTEM RESPONSE
PBSE DETECTOR
RELATIVE SYSTEM RESPONSE
1.0
0.8
0.6
0.4
0.2
0.0
17000.0
20000.0
23000.0
26000.0
29000.0
32000.0
35000.0
38000.0
41000.0
44000.0
47000.0
50000.0
WAVENUMBERS (CM-1)

FIGURE IV-3.1

SURVEY SPECTRUM OF FLAT FLAME
RESOLUTION= 0.25CM^{-1}
NUMBER OF SCANS= 256
CH_4 :AIR MIX RATIO= 1:7

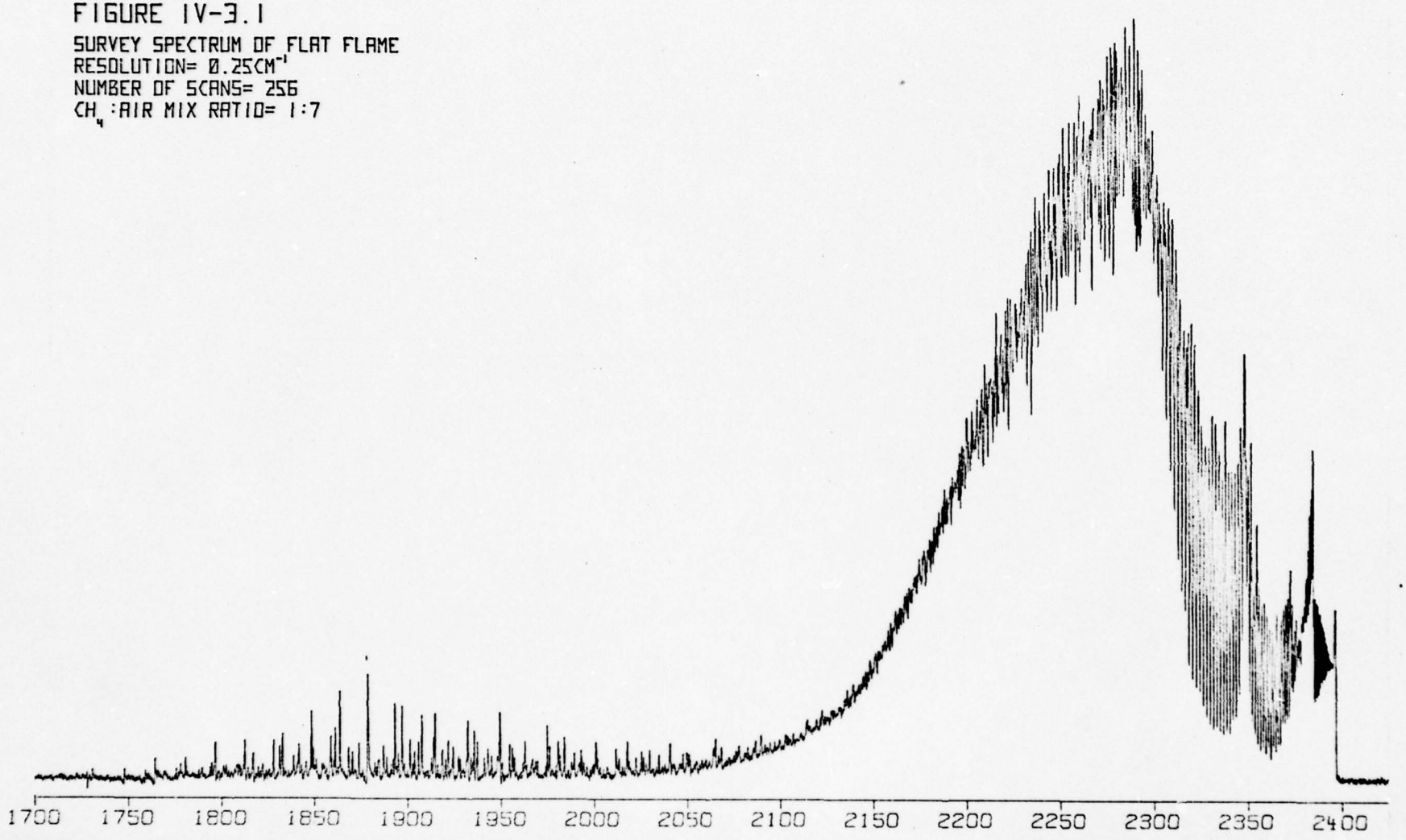

FIGURE IV-3.2

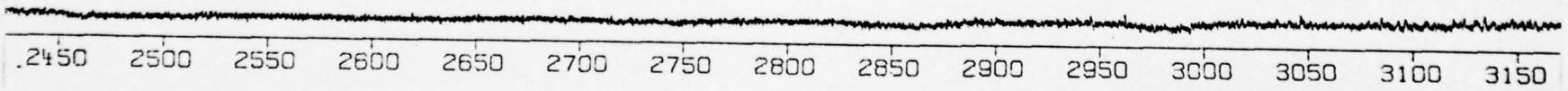
.2450
2500
2550
2600
2650
2700
2750
2800
2850
2900
2950
3000
3050
3100
3150

FIGURE IV-3.3

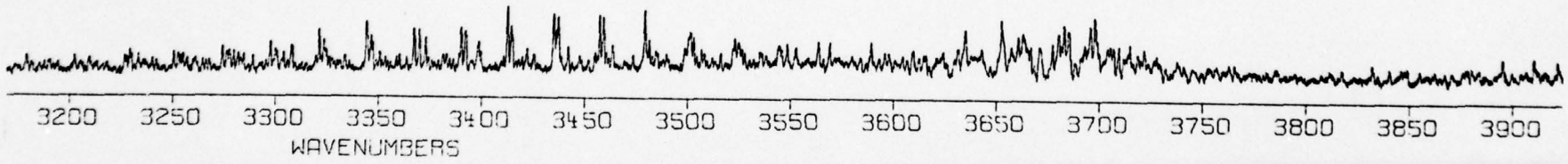
3200
3250
3300
3350
3400
3450
3500
3550
3600
3650
3700
3750
3800
3850
3900
WAVENUMBERS

FIGURE IV-3.4

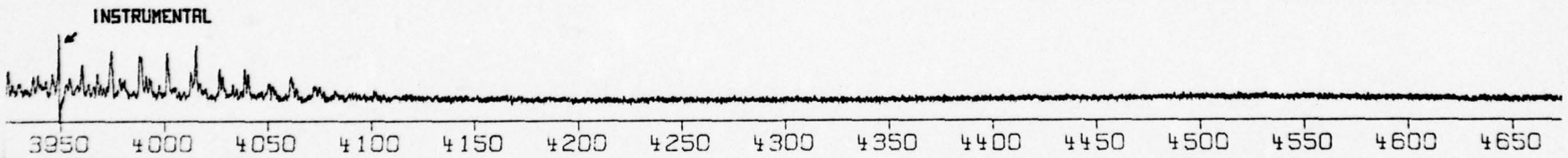
INSTRUMENTAL
3950
4000
4050
4100
4150
4200
4250
4300
4350
4400
4450
4500
4550
4600
4650

b) CO_2 emission from 2050cm^{-1} to 2400cm^{-1} c) H_2O and CO_2 from 3200cm^{-1} to 4100cm^{-1}.[12] Figures IV-1 and IV-2 should be kept in mind while considering figure IV-3. The H_2O emission between 1700cm^{-1} and 2050cm^{-1} occurs in a region of relatively strong atmosphere absorption and relatively poor detector response, therefore the intensity of the band is considerably greater than it appears on the plot. Similar arguments apply for the H_2O and CO_2 bands from 3200cm^{-1} to 4100cm^{-1}. Atmospheric absorption is also present in the region from 2300cm^{-1} to 2380cm^{-1} in the region of CO_2 emission; however, in the regions from 2050cm^{-1} to 2300cm^{-1} and from 2380cm^{-1} to 2400cm^{-1} there is little absorption. The lower frequency H_2O emission results from transitions involving a change of one quantum of the V_2 normal mode frequency, i.e. $\Delta v_2=1$.[11] The CO_2 emission in the vicinity of 2300cm^{-1} results from transitions involving a change of one quantum of asymetric stretch, i.e. $\Delta v_3=1$.[11,12] The density of lines in this region is so great that the line spacing is less than the doppler width of the lines,[12] therefore the feature appears to be almost a continium with fine structure superimposed on it. Two band heads can be seen at 2384 cm^{-1} and 2397cm^{-1} resulting from the $01^{1}1 \rightarrow 01^{1}0$ and $00^{0}1 \rightarrow 00^{0}0$ transitions.[13] The H_2O and CO_2 emission in the high frequency region results from a number of transitions; however, the

stronger one for H_2O are $\Delta v_1=1$, $\Delta v_3=1$, and $\Delta v_2=2$ and for CO_2, the combination bands $\Delta v_1=1 + \Delta v_3 = 1$ and $\Delta v_2 = 2 + \Delta v_3 = 1$.[11]

B. Emission from Different Zones - Figures IV-4 through IV-8 show the spectra obtained at various heights above the burner base. The emitting region has a height of about 1.5mm, except for the region at the burner base, where the base acts as an additional stop in the collection optics, reducing the height of the region to about .75mm. The CH_4: Air ratio was 1:7 by volume in all of the data. Only the spectral region from $1700cm^{-1}$ to $2400cm^{-1}$ is plotted, as the remaining regions showed little change. The resolution in all the plots is $1cm^{-1}$. While the vertical scale is arbitrary, comparisons can be made between plots in this series as factors such as system gain, number scans, etc. was constant. Due to the smaller emitting volume at the burner base, the vertical scale in figure IV-4 is expanded by 2 over the remaining plots. An interesting feature in the plots is the appearance of lines from the CO fundamental in the data near the base of the burner. The structure extends from about 2000 cm^{-1} to $2250cm^{-1}$ and results primarily from the $1 \rightarrow 0$ transition.[14] The CO emission drops off very quickly above the base indicating combustion is going to completion very rapidly. This is consistent with mass spectrometer data from Battelle Laboratories showing CO concentration going to zero approxi-

FIGURE IV-4

SPECTRUM FROM BURNER BASE
METHANE:AIR MIX= 1:7
RESOLUTION= 1CM^{-1}
NUMBER OF SCANS= 256

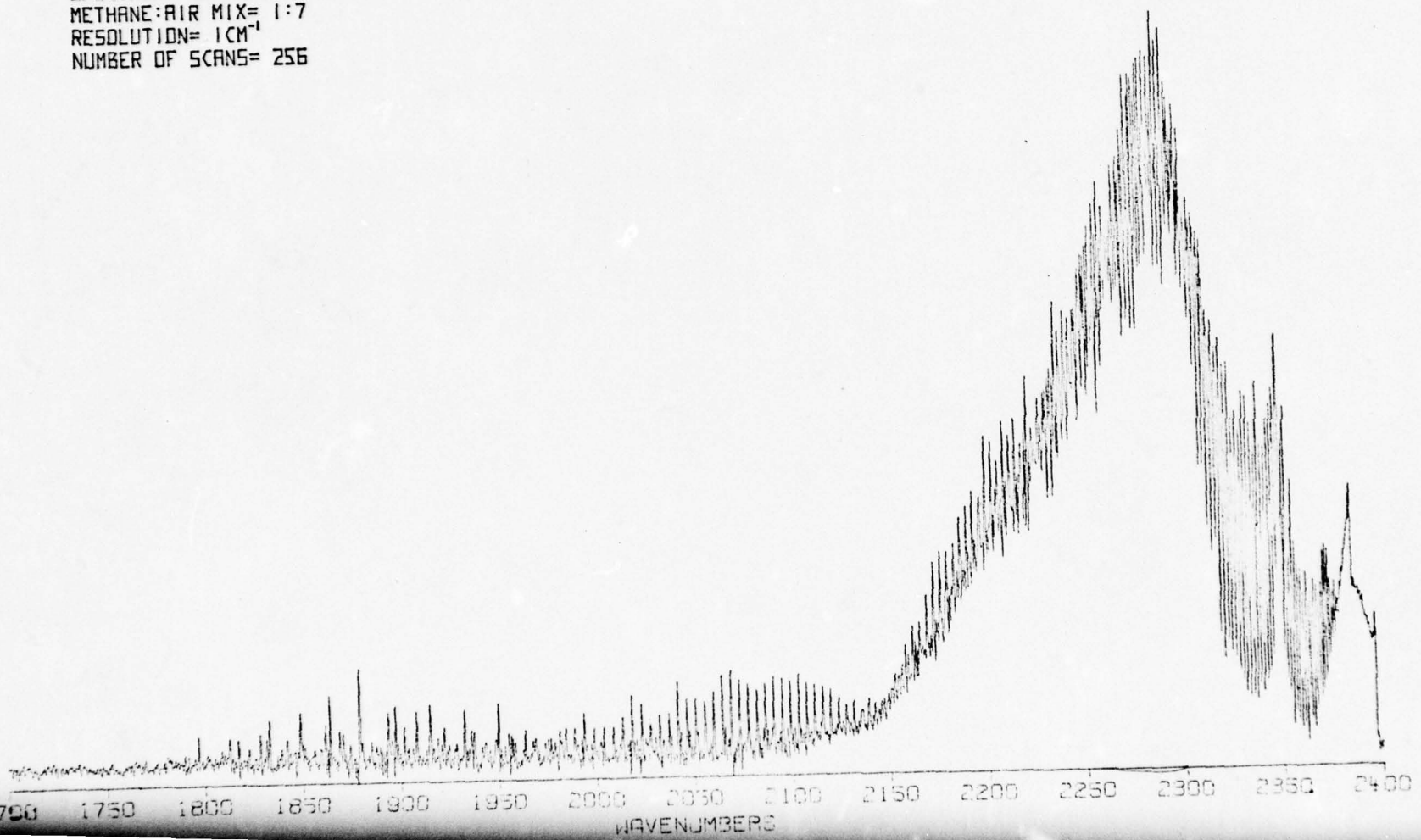

FIGURE IV-5

SPECTRUM FROM 2MM. ABOVE BURNER BASE
METHANE:AIR MIX= 1:7
RESOLUTION= $1CM^{-1}$
NUMBER OF SCANS= 256

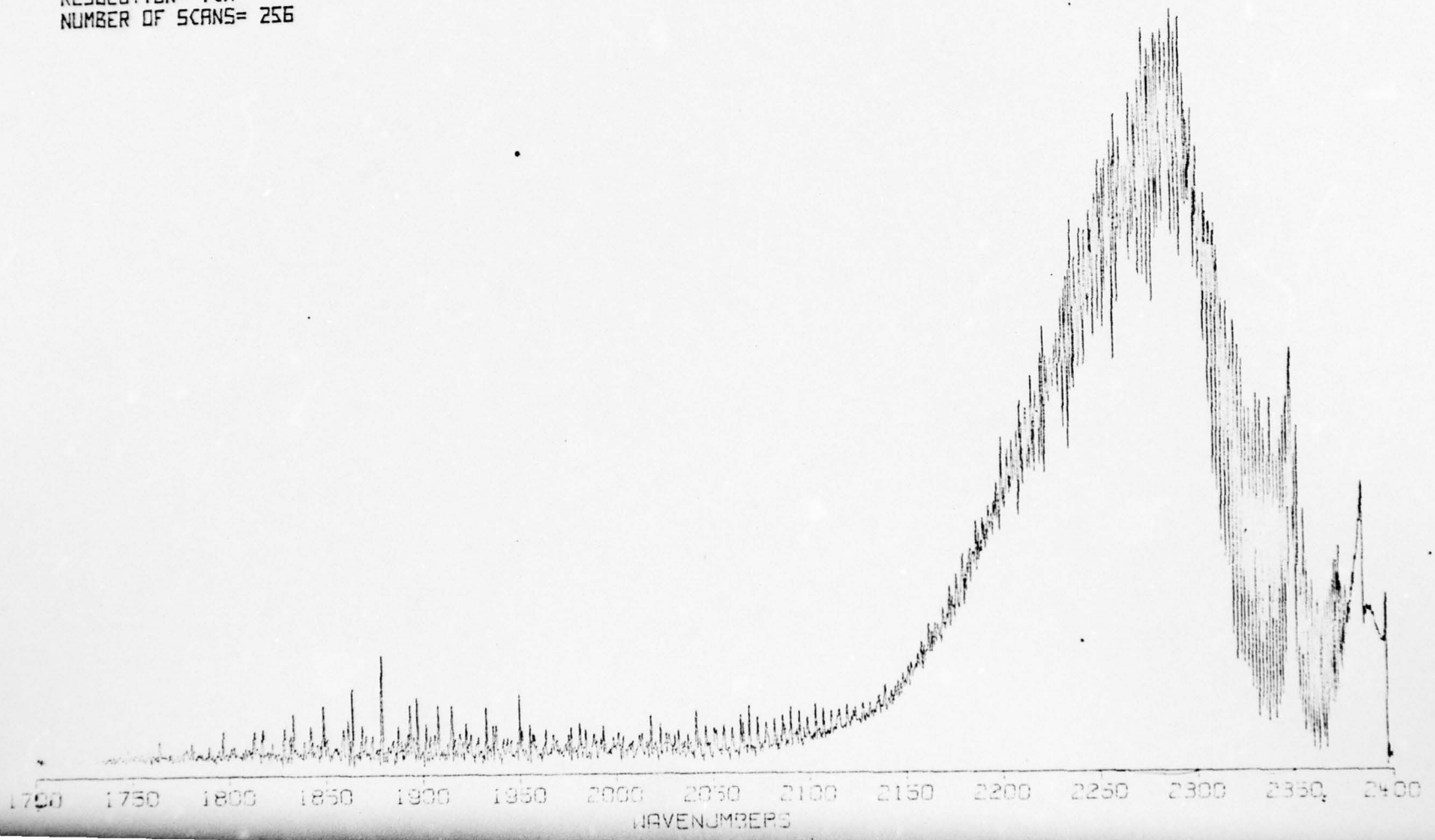

FIGURE IV-6

SPECTRUM FROM 4MM. ABOVE BURNER BASE
METHANE:AIR MIX= 1:7
RESOLUTION= $1CM^{-1}$
NUMBER OF SCANS= 256

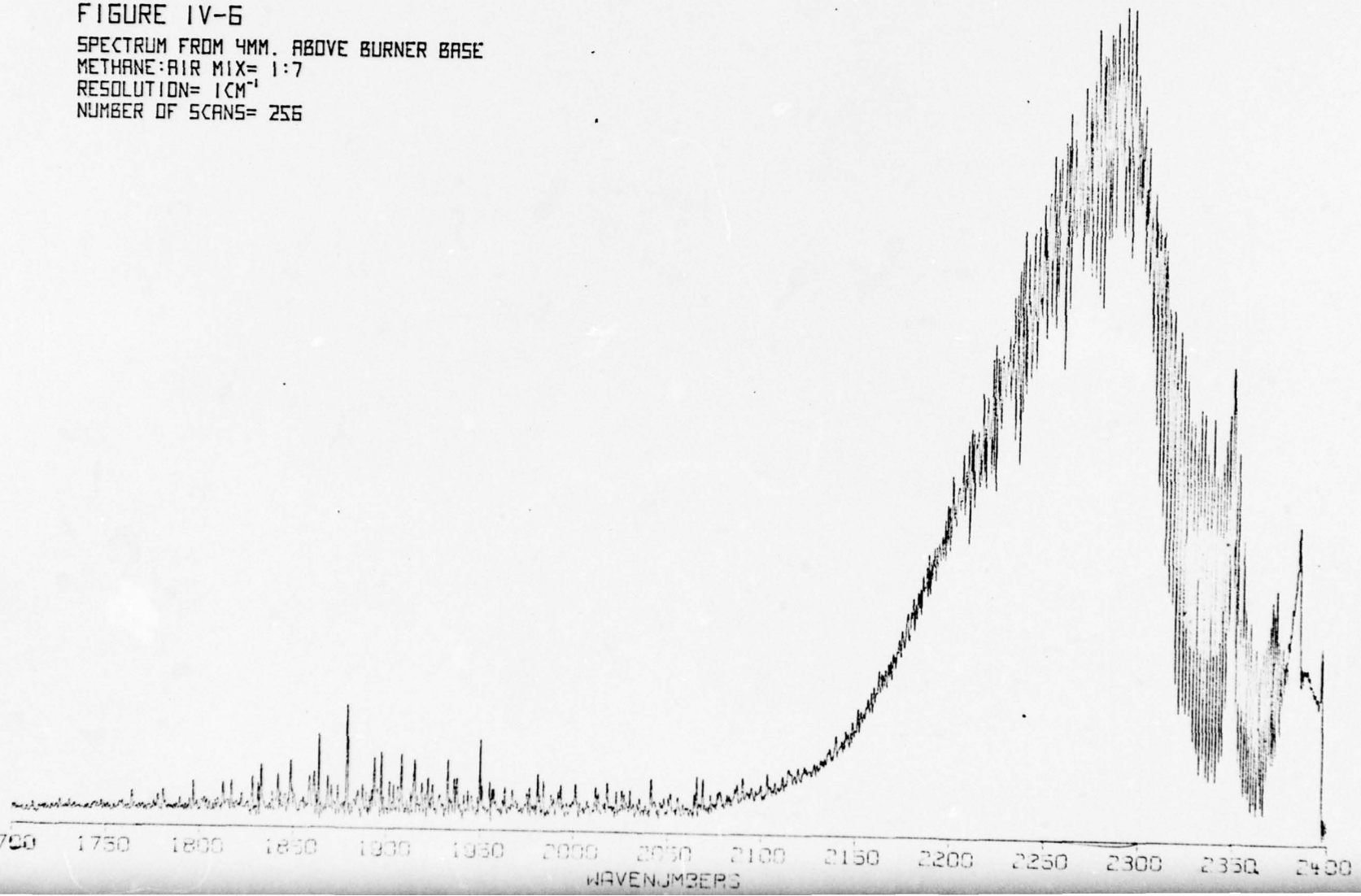

FIGURE IV-7

SPECTRUM FROM 6MM. ABOVE BURNER BASE
METHANE:AIR MIX= 1:7
RESOLUTION= $1CM^{-1}$
NUMBER OF SCANS= 256

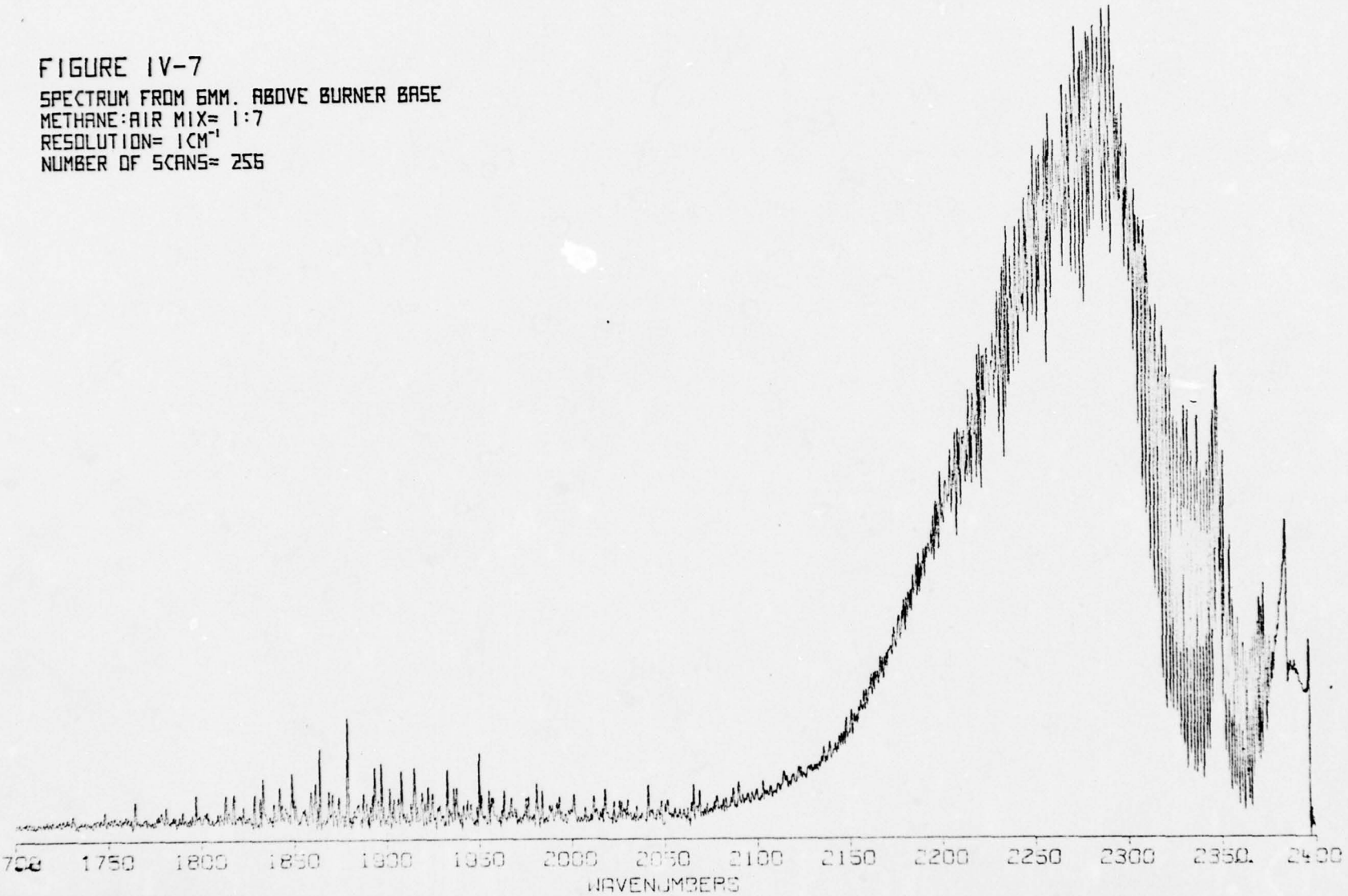

FIGURE IV-B

SPECTRUM FROM 8MM. ABOVE BURNER BASE
METHANE:AIR MIX= 1:7
RESOLUTION= 1CM^{-1}
NUMBER OF SCANS= 256

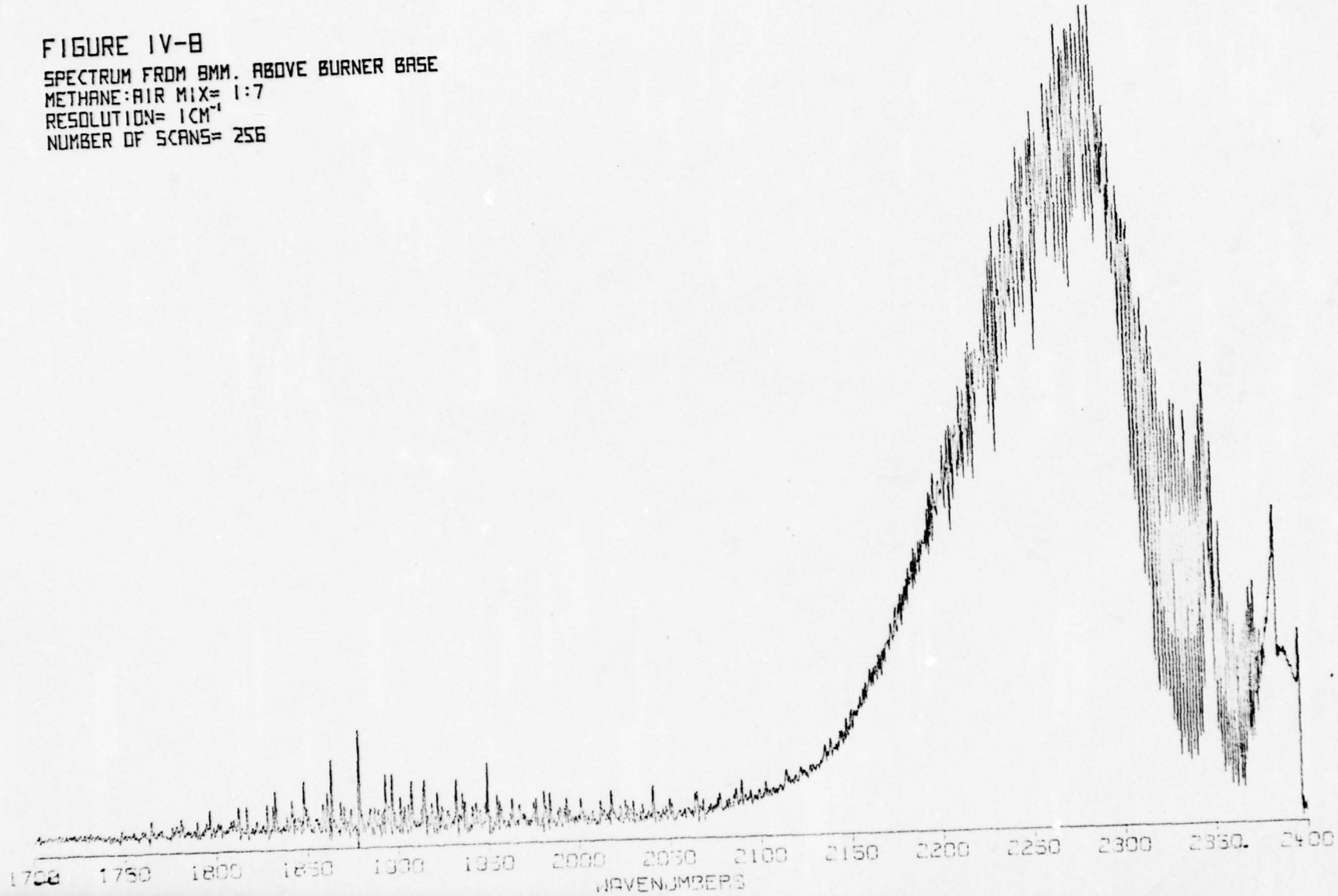

mately 5mm above the burner base for a 1/10 atmosphere flame.[15] At atmosphere the combustion is expected to occur more rapidly, thus the CO concentration should drop off even faster in our case. No CO overtone spectrum was observed in any of the data.

C. Variation of Mix Ratio - Figures IV - 9 through IV - 12 show spectra oblained with rich CH_4 - Air mixtures ranging from 1:3.4 to 1:5.8 by volume. All data was taken at a height above the burner base of 10mm. As in part B), intensity comparisons among the plots can be made. The resolution was $1cm^{-1}$. Again, CO emission is observed between $2000cm^{-1}$ and $2050cm^{-1}$, for mix ratios less than approximately 5:1. In this data, $2 \rightarrow 1$ transitions can be seen along with the $1 \rightarrow 0$. No methane bands could be identified in any of the data, nor could any CO overtone bands be seen.

D. High Resolution Spectra - Figures IV - 13, 14 and 15 show spectra taken with $.06cm^{-1}$ resolution in the region $1700cm^{-1}$ to $2400cm^{-1}$ under two sets of experimental parameters. Figures IV - 13 and IV - 14 were obtained from a region of the flame just above the burner base with a "normal" 1:7 CH_4:Air mix, while figure IV - 15 was obtained at a height of 6mm above the burner base with a rich 1:3.9 CH_4:Air mix. Figure IV - 14 is a detail plot of the rotational structure near the $00^{\circ}1 \rightarrow 00^{\circ}0$ band head of CO_2. By comparing the spec-

FIGURE IV-9.1

METHANE:AIR MIX= 1:3.4 -RICH FUEL MIX
SPECTRUM FROM 10MM. ABOVE BURNER BASE
RESOLUTION= $1CM^{-1}$
NUMBER OF SCANS= 256

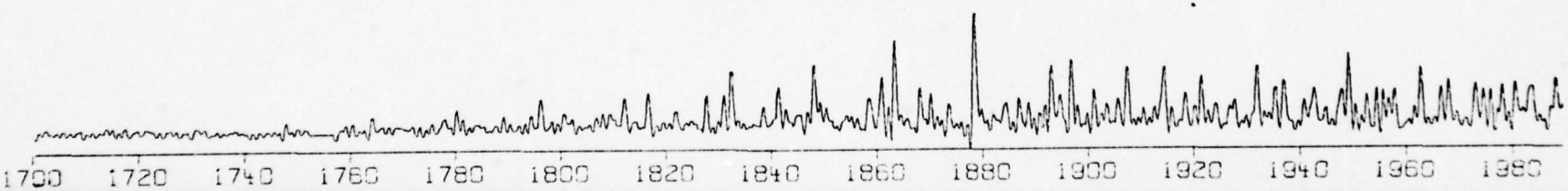

FIGURE IV-9.2

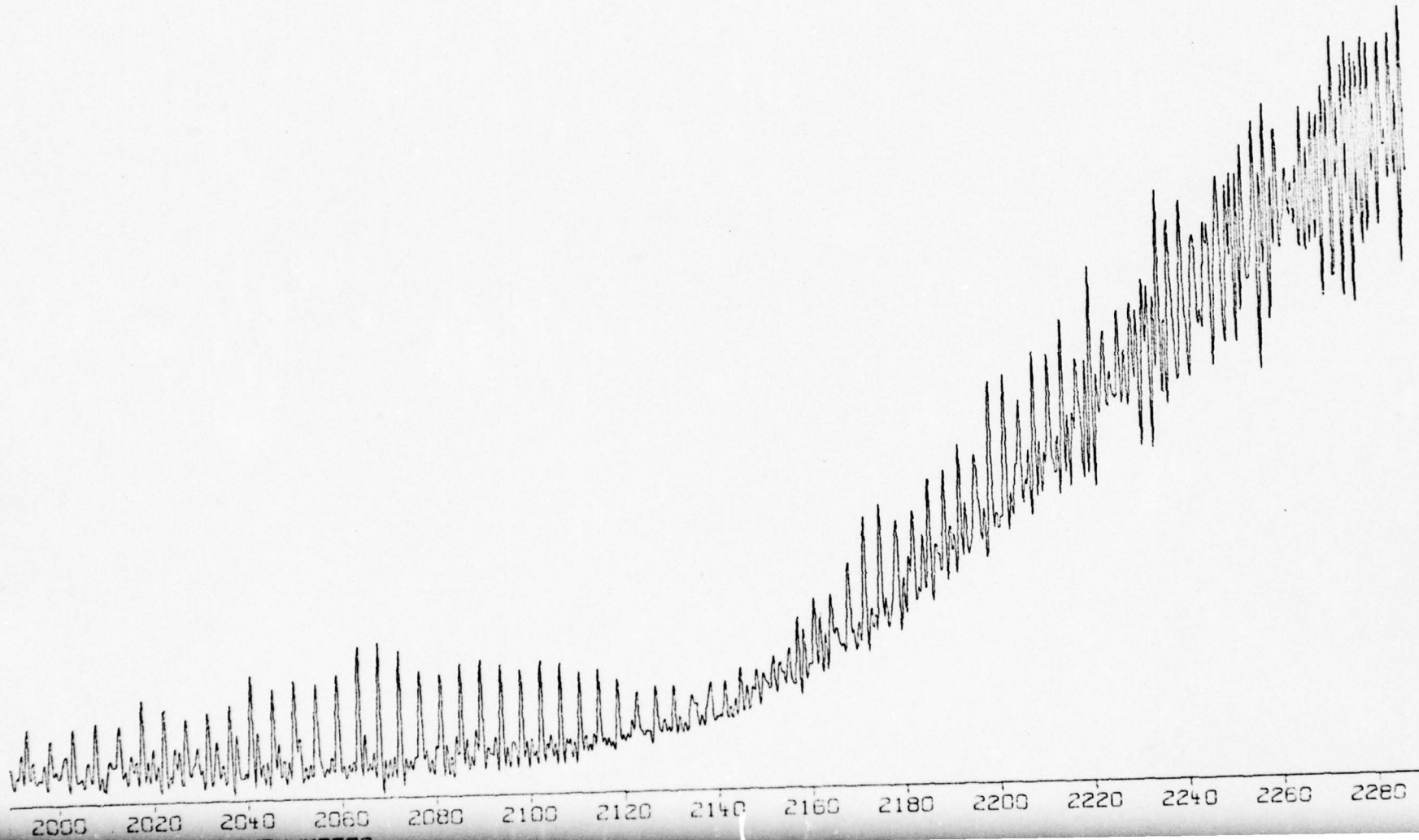
2000
2020
2040
2060
2080
2100
2120
2140
2160
2180
2200
2220
2240
2260
2280

FIGURE IV-9.3

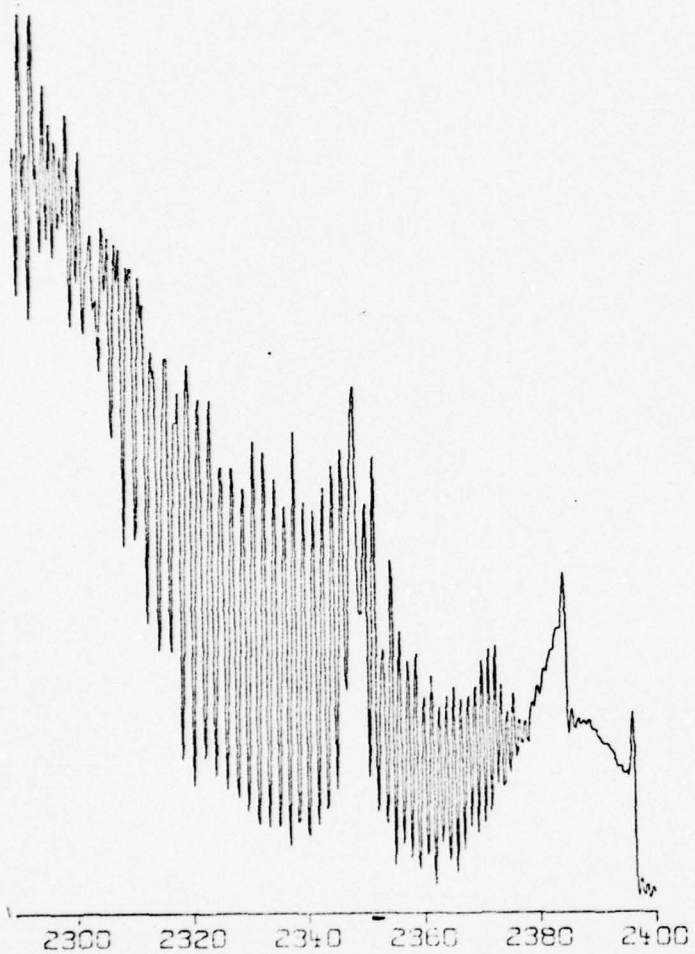

FIGURE IV-10.1

METHANE:AIR MIX= 1:3.9 -RICH FUEL MIX
SPECTRUM FROM 10MM. ABOVE BURNER BASE
RESOLUTION= $1CM^{-1}$
NUMBER OF SCANS= 256

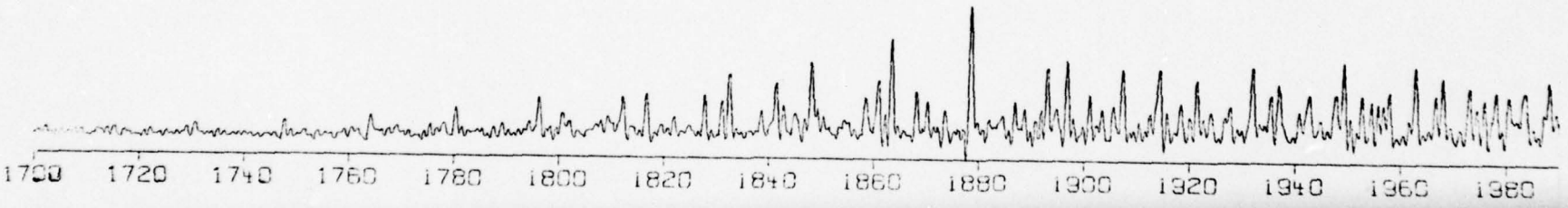

FIGURE IV-10.2

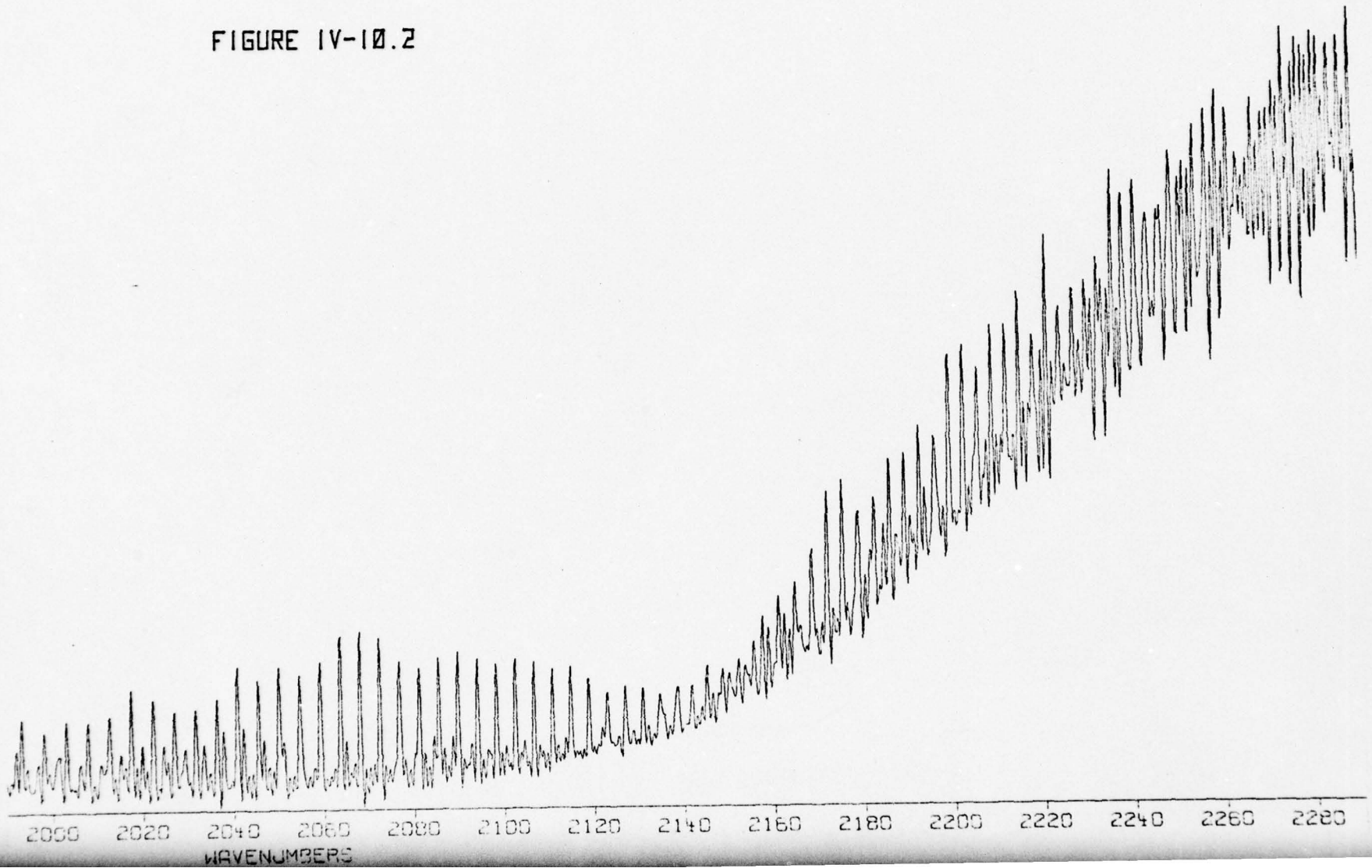

FIGURE IV-10.3

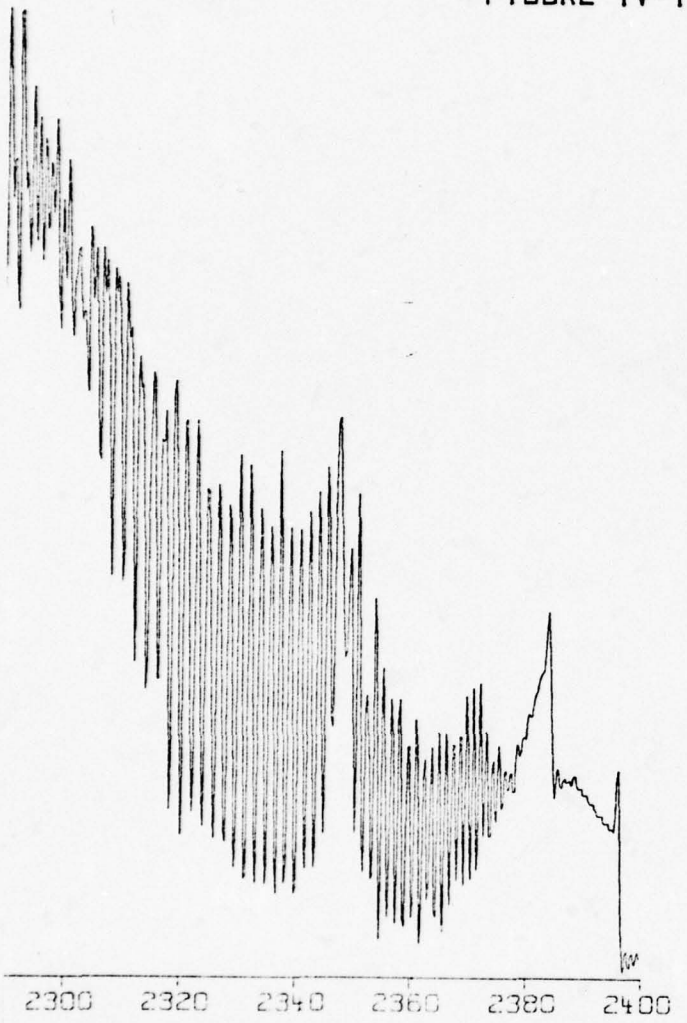

FIGURE IV-11.1

METHANE:AIR MIX= 1:5.8 -RICH FUEL MIX
SPECTRUM FROM 10MM. ABOVE BURNER BASE
RESOLUTION= 1CM^{-1}
NUMBER OF SCANS= 256

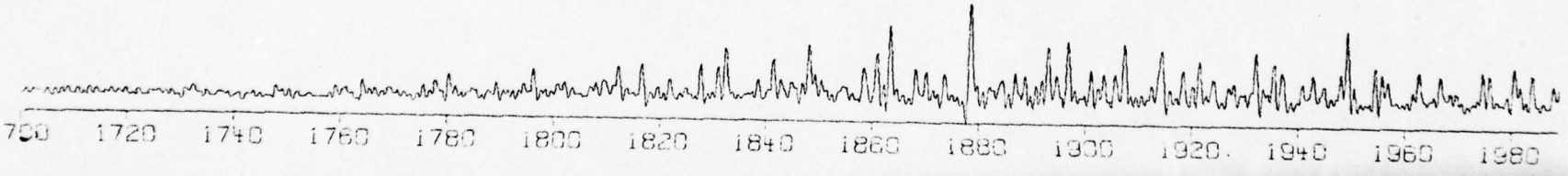

FIGURE IV-11.2

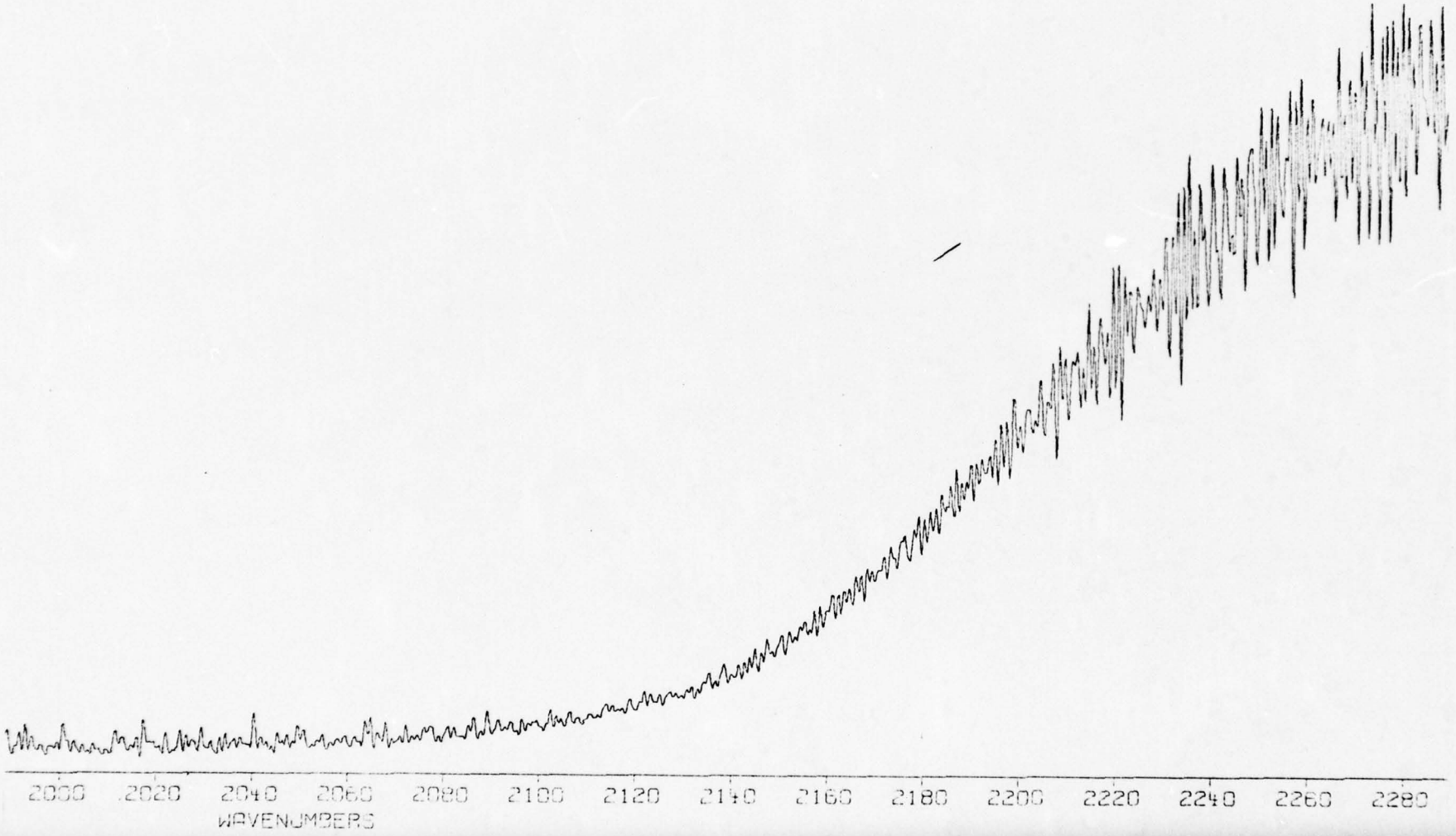

FIGURE IV-11.3

FIGURE IV-12.1

METHANE:AIR MIX= 1:4.8 -RICH FUEL MIX
SPECTRUM FROM 10MM. ABOVE BURNER BASE
RESOLUTION= $1CM^{-1}$
NUMBER OF SCANS= 256

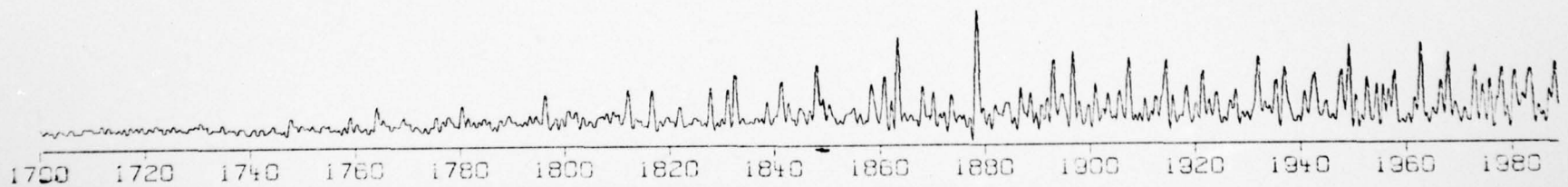

FIGURE IV-12.2

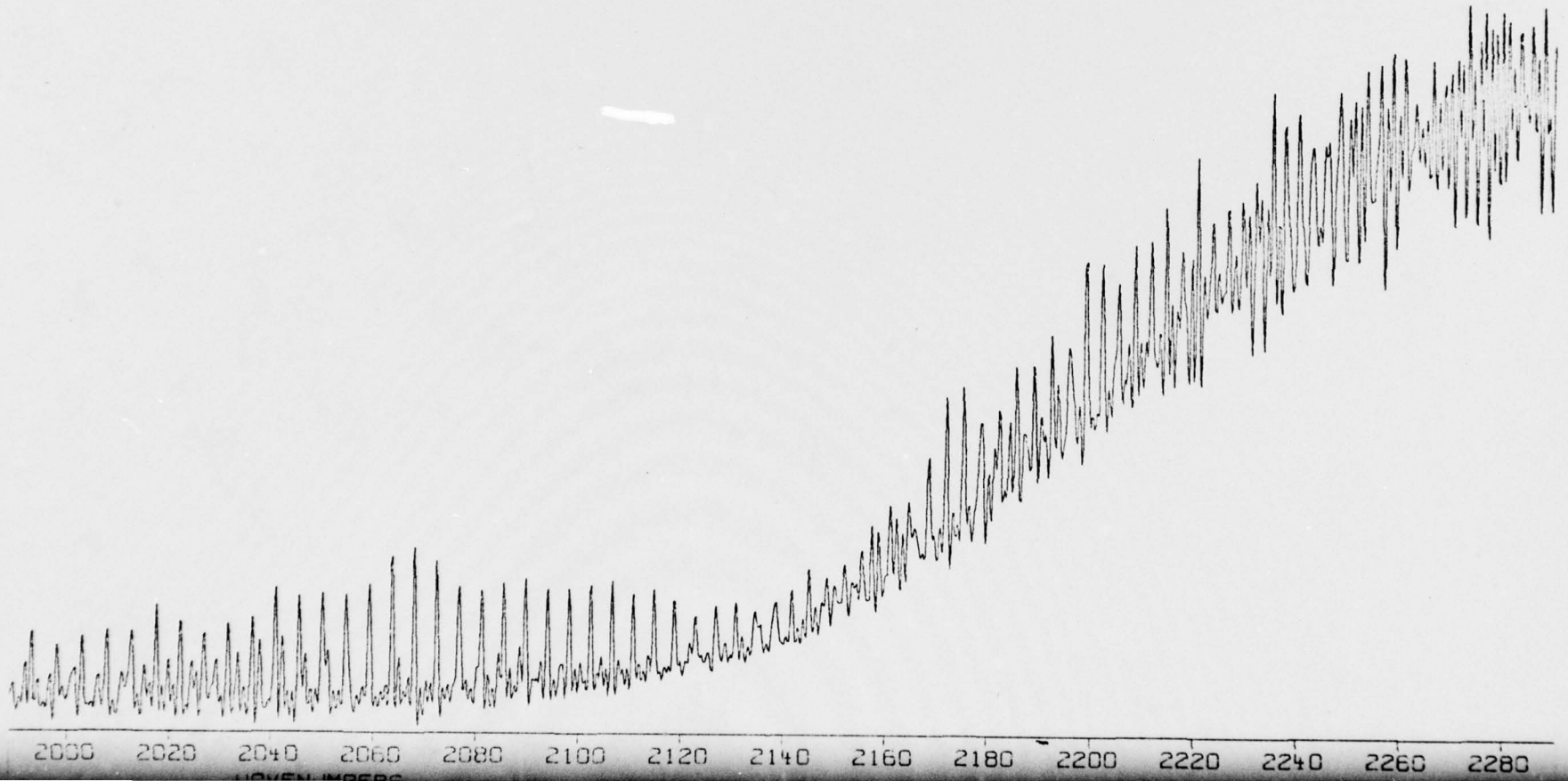

FIGURE IV-12.3

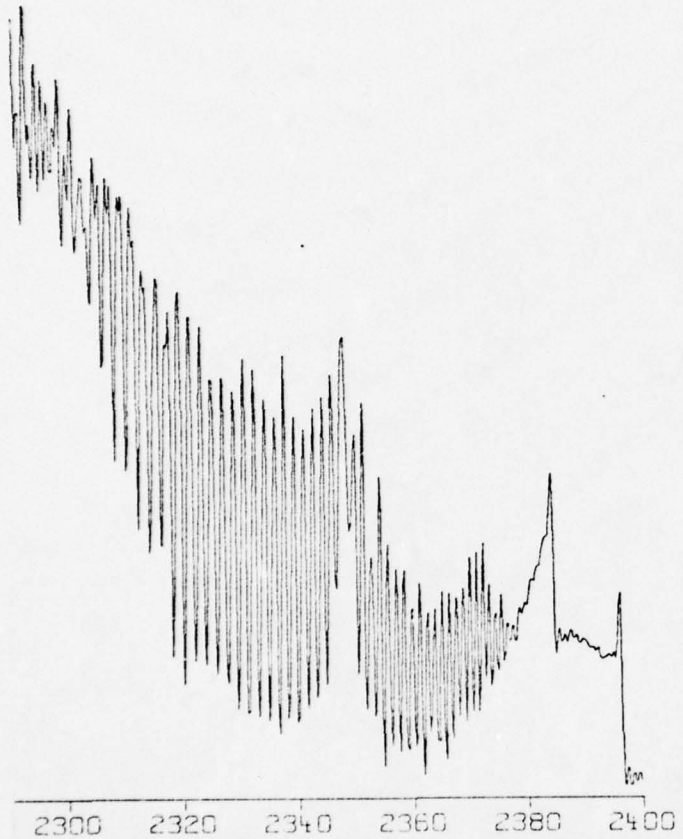

FIGURE IV-13.1

HIGH RESOLUTION SPECTRUM
RESOLUTION= 0.05CM^{-1}
SPECTRUM FROM BURNER BASE
METHANE:AIR MIX= 1:7
NUMBER OF SCANS= 256

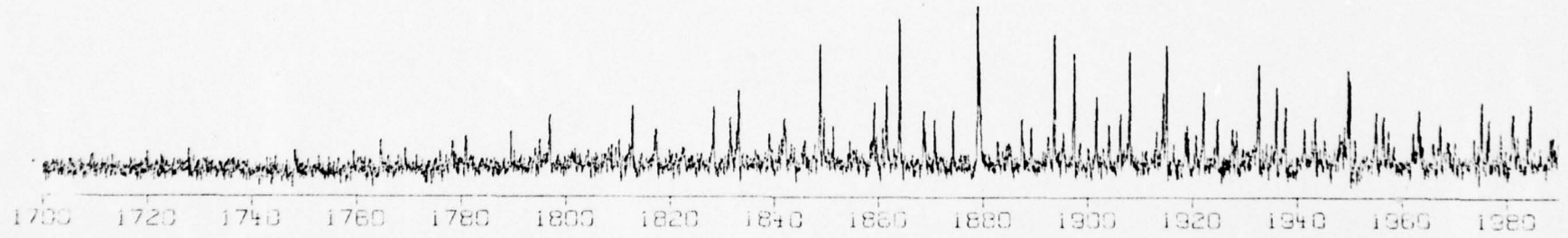

FIGURE IV-13.2

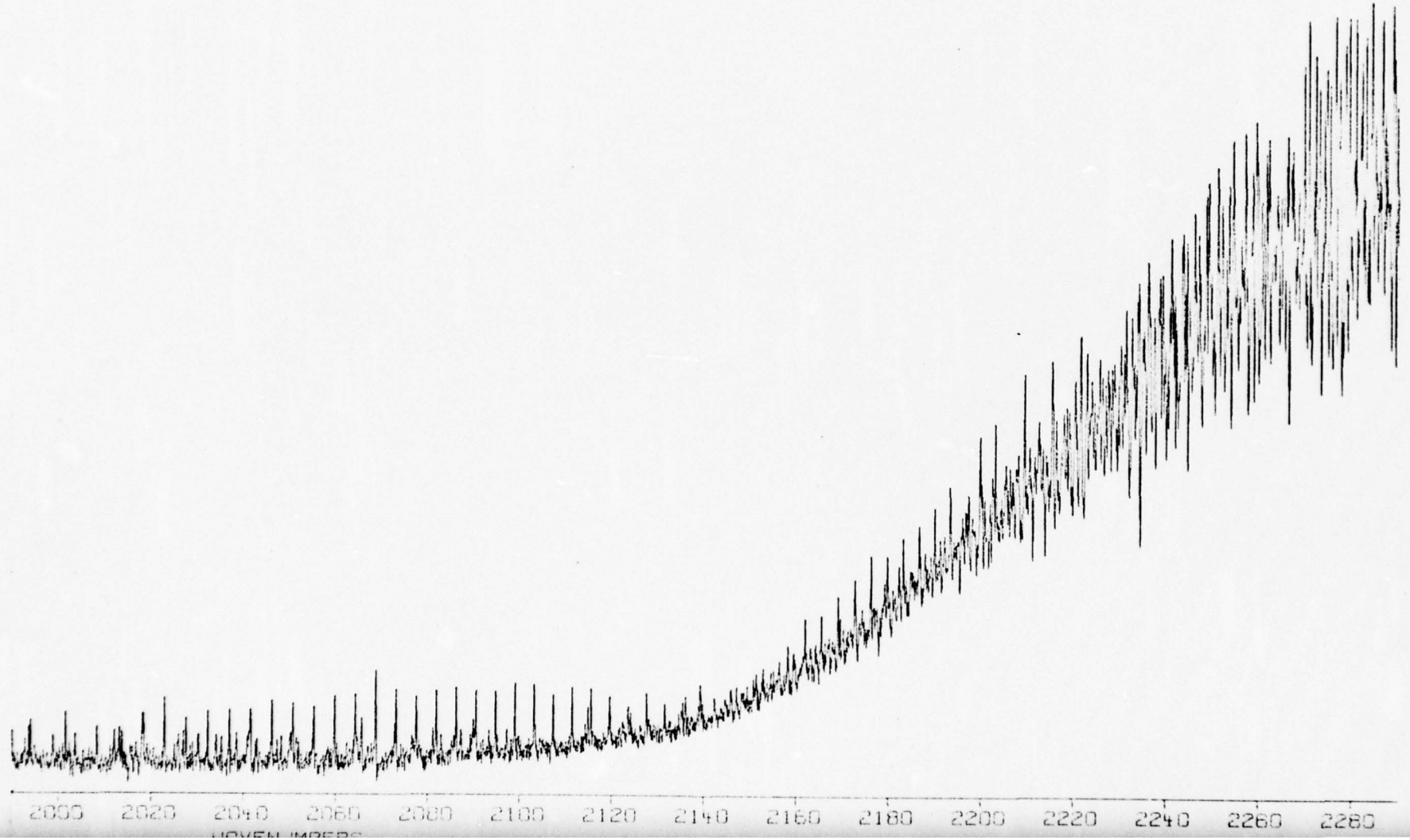

FIGURE IV-13.3

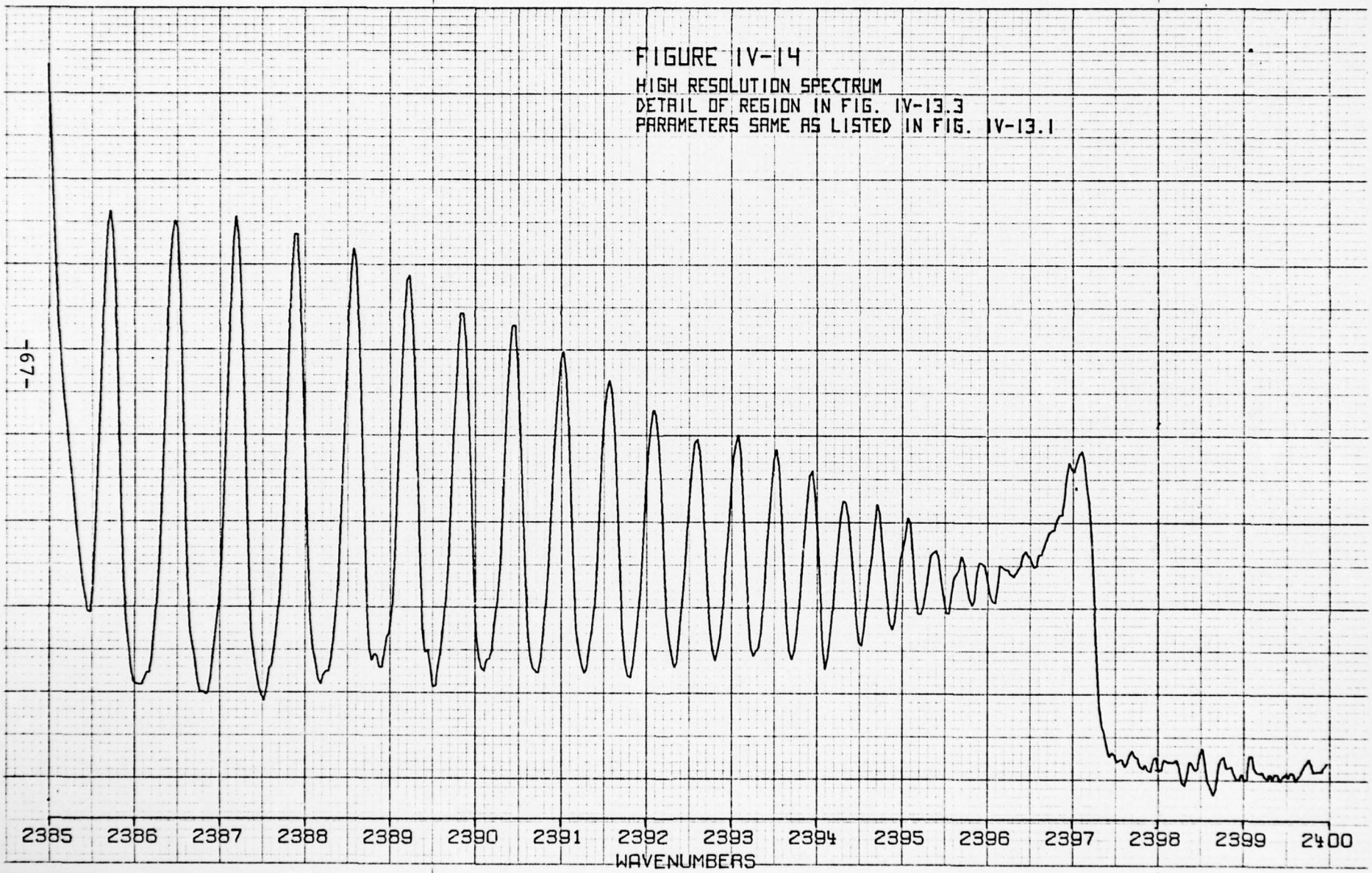

FIGURE IV-14
HIGH RESOLUTION SPECTRUM
DETAIL OF REGION IN FIG. IV-13.3
PARAMETERS SAME AS LISTED IN FIG. IV-13.1

FIGURE IV-15.1

HIGH RESOLUTION SPECTRUM
RESOLUTION= 0.06CM^{-1}
SPECTRUM FROM 6MM. ABOVE BURNER BASE
METHANE:AIR MIX= 1:3.9 -RICH FUEL MIX
NUMBER OF SCANS= 256

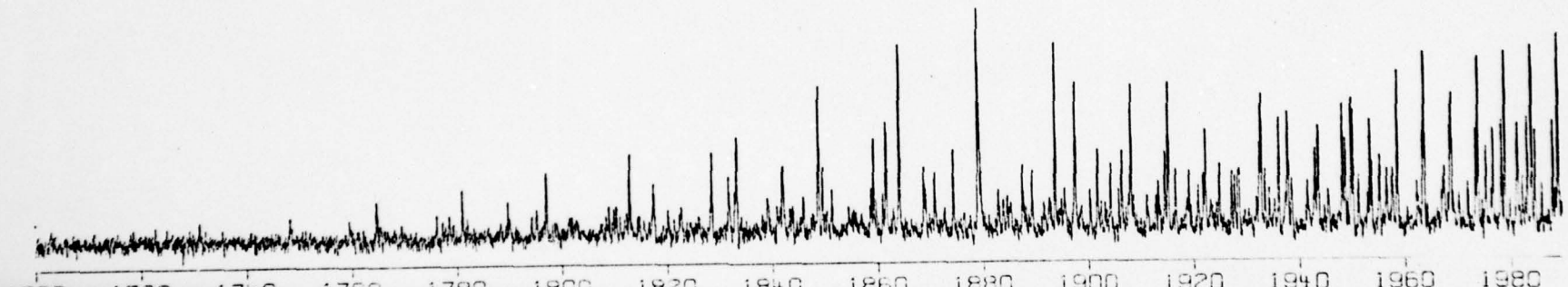

FIGURE IV-15.2

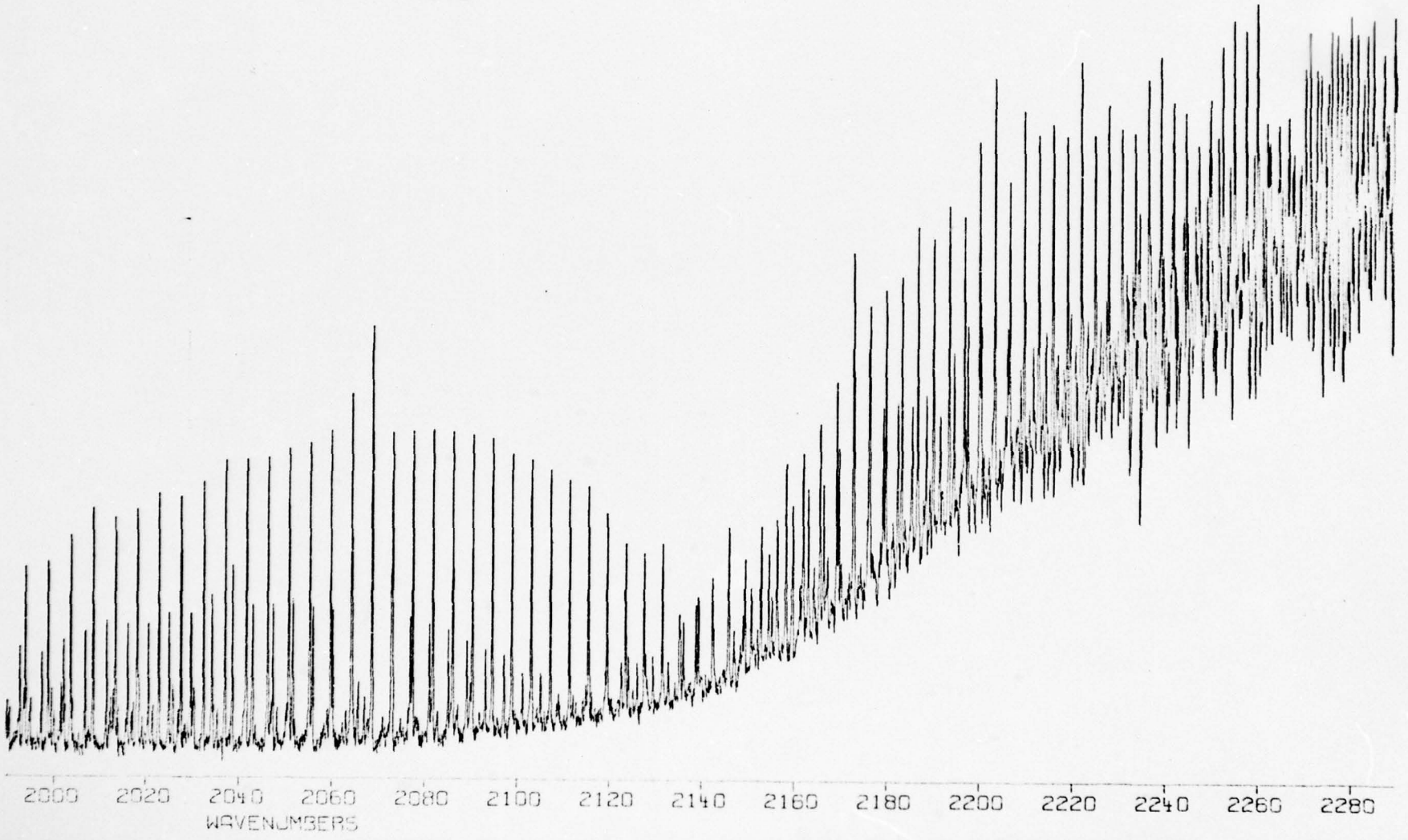

FIGURE IV-15.3

tra with those of Pyler, et al.[13] it is found that J" values up to 102 are observed. In both figures IV - 13 and IV - 15 it is clear that the CO_2 line density in the region from roughly 2100cm^{-1} to 2300cm^{-1} is too great to allow individual lines to be resolved at this temperature and pressure. Emission from the CO fundamental band can be seen in both figures.

E. Data Below 1700cm^{-1} - Some preliminary results were obtained in the region from about 400cm^{-1} to 1700cm^{-1}, with roughly 1cm^{-1} resolution, using the TGS detector and the KB_r beamsplitter. A sample of the spectra is shown in figure IV - 16. As discussed earlier, the poor performance of the TGS made data aquisition in the region very difficult, thus only one set of parameters was used. The CH_4:Air mix was 1:7 and the region of the flame sampled was 6mm above the burner base. The additional features below 1700cm^{-1} are premarily the 15um band of CO_2 (in the vicinity of 670cm^{-1}) and more of the 6.3um band of H_2O (in the vicinity of 1600cm^{-1}).

F. Rotational Temperature Determination - The rotational temperature of CO in a rich 1:3.9 CH_4:Air mixture was calculated from the relative intensities of the rotational lines of the fundamental from the data in figure IV - 15. The intensity of a rotational emission line from a given vibrational level can be written as [14]

$$I_{J',J"} = \frac{2N\nu^4}{Q_r} S_{J"} \mathrm{Exp}[-F(J')hc/kT] \qquad \text{IV - 1}$$

FIGURE IV-16

DATA IN THE REGION BELOW 1700CM^{-1}
KBR BEAMSPLITTER/TGS DETECTOR
METHANE:AIR MIX= 1:7

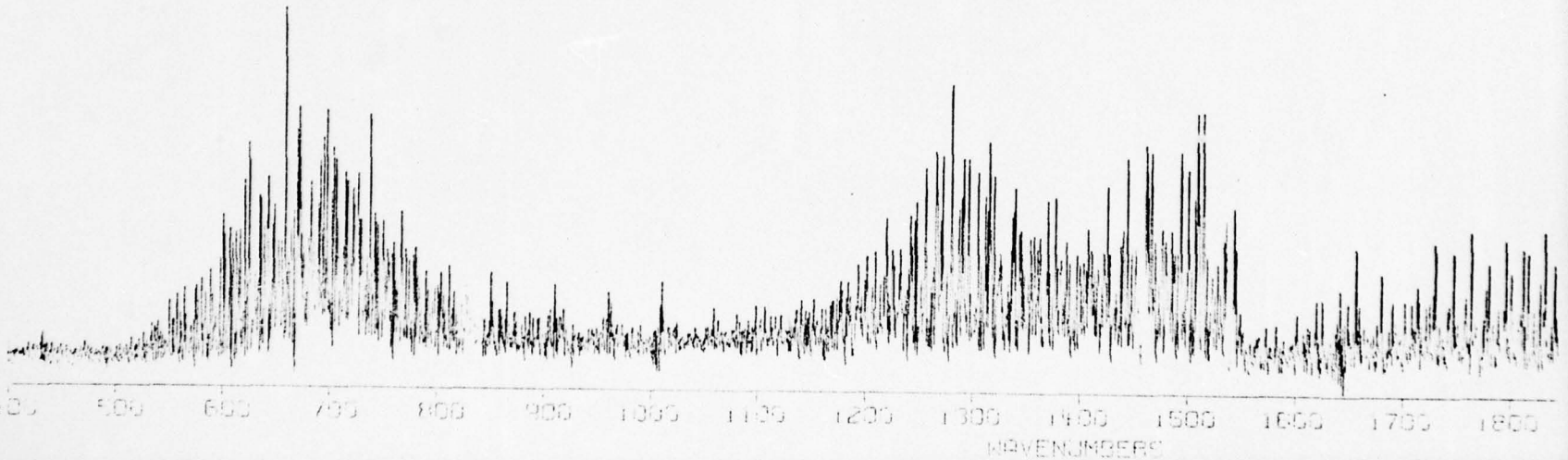

where N is a constant for the given vibrational level, ν is the wavenumber of the line, Q_r is the rotational partition function, F(J') is the rotational term value of the upper level, h is Planck's constant, c is the speed of light, k is Boltzmann's constant, and T is the rotational temperature. $S_{J"}$ is the part of the square of the transition moment that depends on J and is given by:

$$S_{J"} = J" + 1 \quad \text{for } \Delta J = +1$$
$$S_{J"} = J" \quad \text{for } \Delta J = -1.$$

The procedure used to determine N and T was to fit the measured relative intensities of a series of rotational lines, from a given vibrational level, to equation IV - 1 using a non-linear least squares adjustment due to Marquardt.[16] Therefore, each vibrational band of the fundamental that could be observed yielded a rotational temperature. Due to interference from CO_2 emission, only P branch lines were used which ranged in wavenumber from 1972cm^{-1} to 2056cm^{-1}. Since the wavenumber range was limited, no correction was made for system sensitivity. Line identification was made by comparing measured lines with lines calculated from the constants of Mantz, et al.[17], and lines identified as consisting of unresolved, multiple lines were not used in the calculation. By comparing the fuel rich spectrum with a

"normal" mix spectrum, CO lines which overlapped H_2O lines were also excluded from the calculation. Thirty seven lines remained in the P branch which were judged sufficiently interference free to be used in the calculation. Figure IV-17 is a sample of the line identification procedure used. Lines were coarsely identified on the plot by computer, then were checked for interference from higher vibrational levels using tables constructed from the constants of ref. 17. Due to the size of the source, line positions were only measured to .03cm^{-1} accuracy. Resolution was less than the half widths of the lines.

The temperature calculated from the three lower vibrational levels observed are given below.

V"=0 ; T = 2199 $\pm$ 160 °K

V"=1 ; T = 1936 $\pm$ 53 °K

V"=2 ; T = 1958 $\pm$ 86 °K

The errors shown are the estimates of the standard deviations from the least squares routine. Since the data was not corrected for self absorption, the temperature determined from the 1 → 0 vibrational band is expected to be in error by the largest amount, probably by more than the 160°K estimated. The weighted average of the three values was calculated using the estimated standard deviations which yielded;

T(weighted average) = 1961°K

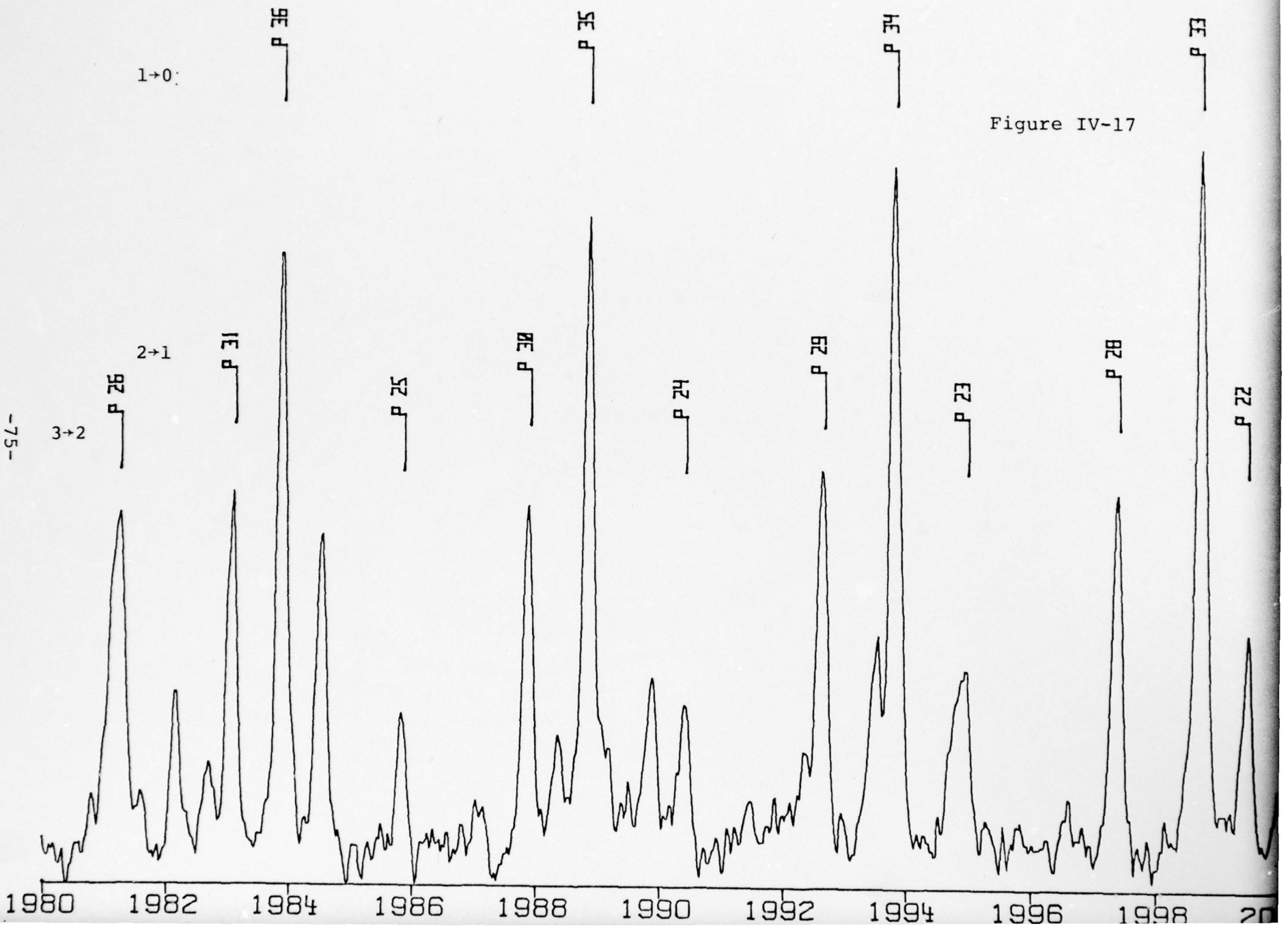
1→0
2→1
3→2
P 36
P 35
P 34
P 33
P 31
P 30
P 29
P 28
P 26
P 25
P 24
P 23
P 22
1980
1982
1984
1986
1988
1990
1992
1994
1996
1998

Figure IV-17

The estimated error in the temperature was taken to be the average of the upper two levels' standard deviations since the error in the V"=0 temperature is probably largely due to self absorption and not statistical fluctuations. The constants N(0), N(1), and N(2) were determined to be;

$$N(0) = 5.00E - 13 \pm 2E - 16$$

$$N(1) = 2.35E - 13 \pm 6E - 17$$

$$N(2) = 9.60E - 14 \pm 6E - 17$$

where the units are arbitrary. Using the average rotational temperature and the calculated constants, the resultant line intensities for the three bands were calculated and are listed in table IV-1. Also listed are the calculated wavenumbers, the measured intensities, the percent difference between calculated and measured intensities, and the line designations. As mentioned earlier, all lines are P branch lines. Assuming the rotational temperature is a reasonable measure of the gas kinetic temperature, the average temperature agrees well with measured values from Battell.[15]

It should be noted that the values of N(0), N(1), and N(2) should yield information about the relative vibrational level populations. Since $S_{J"}$ is the J - dependent part of the square of the transition moment, the constants N(v") can be written,[14]

$$N(v") = W\, n(v') \left| R^{v',v"} \right|^2 \qquad \text{IV-2}$$

Table IV-1

Wavenumber (cm^{-1})	Designation (v",J")	Intensity Meas. (arb. units)	Intensity Calc. (arb. units)	Percent Diff.
1971.98	(2,28)	4.210E-02	4.062E-02	3.51
1978.31	(1,32)	9.249E-02	8.305E-02	10.21
1978.93	(0,37)	1.459E-01	1.270E-01	12.92
1983.13	(1,31)	9.463E-02	8.848E-02	6.50
1983.94	(0,36)	1.531E-01	1.380E-01	9.88
1985.88	(2,25)	4.202E-02	4.617E-02	9.88
1987.92	(1,30)	9.212E-02	9.391E-02	1.94
1988.91	(0,35)	1.529E-01	1.493E-01	2.34
1990.45	(2,24)	4.459E-02	4.777E-02	7.13
1993.86	(0,34)	1.733E-01	1.610E-01	7.09
1994.99	(2,23)	5.344E-02	4.920E-02	7.94
1997.42	(1,28)	9.566E-02	1.045E-02	9.28
1998.78	(0,33)	1.779E-01	1.730E-01	2.77
1999.50	(2,22)	6.233E-02	5.043E-02	19.09
2002.11	(1,27)	1.065E-01	1.096E-01	2.93
2003.67	(0,32)	2.035E-01	1.851E-01	9.03
2003.98	(2,21)	5.282E-02	5.145E-02	2.60
2006.78	(1,26)	1.145E-01	1.145E-01	.02
2011.42	(1,25)	1.244E-01	1.190E-01	4.32
2013.35	(0,30)	2.200E-01	2.096E-01	4.71
2016.03	(1,24)	1.220E-01	1.232E-01	1.00
2017.21	(2,18)	4.800E-02	5.292E-02	10.26
2018.15	(0,29)	2.263E-01	2.218E-01	2.00
2021.56	(2,17)	4.611E-02	5.282E-02	14.55
2022.91	(0,28)	2.378E-01	2.337E-01	1.74
2025.14	(1,22)	1.299E-01	1.302E-01	.25
2027.65	(0,27)	2.376E-01	2.452E-01	3.20
2029.66	(1,21)	1.310E-01	1.329E-01	1.46
2032.35	(0,26)	2.514E-01	2.562E-01	1.91
2034.41	(2,14)	4.731E-02	5.047E-02	6.68
2037.03	(0,25)	2.729E-01	2.666E-01	2.32
2041.67	(0,24)	2.731E-01	2.761E-01	1.10
2043.00	(1,18)	1.401E-01	1.369E-01	2.28
2046.28	(0,23)	2.763E-01	2.847E-01	3.03
2046.98	(2,11)	5.170E-02	4.486E-02	13.22
2050.85	(0,22)	2.854E-01	2.921E-01	2.36
2056.05	(1,15)	1.387E-01	1.337E-01	3.64

where W is a constant, n(v') is the number density of molecules in the v' vibrational level, and $R^{v',v''}$ is the transition moment. For a linear dipole moment function, and $\Delta v=1$, it can be shown from the calculations of Heaps and Herzberg[18] that $|R^{v',v''}|^2$ can be approximated by:

$$|R^{v',v''}|^2 \simeq |R^{1,0}|^2 \cdot \left(\frac{\nu_{1,0}}{\nu_{v',v''}}\right)^2 \cdot v' \qquad \text{IV-3}$$

if $2v' << \frac{W_e}{W_e X_c} - 1$. In equation IV-3 $\nu_{v',v''}$ is the wavenumber for the J"=J'=0 transition. Using equation IV-2 and IV-3, the relative number densities found are:

$$n(2)/n(1) = .229$$

$$n(3)/n(1) = .0609$$

Assuming the vibrational levels follow a Boltzman distribution, the previous ratios would yield a vibrational temperature of;

$$T(\text{vibrational}) = 2115 \pm 50°K.$$

V. Conclusions

FTS can yield rapid, high resolution infrared emission spectra of combustion plasmas over a broad spectral region with high sensitivity, high wavenumber accuracy, and good stray light rejection. If high resolution is not needed, very rapid scanning and processing can be accomplished. Manipulation of stored spectra (background subtraction, wavenumber to wavelength conversion, etc.) can be performed using the same computing equipment needed for fourier transforming the interferograms. Once a particular optical system and detector have been calibrated with a standard blackbody, absolute intensity measurements become routine. Species identification, remote temperature determination, and species concentration determination (if absolute intensities are known) is possible if infrared-active species are present in the plasma. The technique overcomes many of the low signal level problems normally associated with infrared spectroscopy and thus allows the abundant information that exist in the infrared region to be more readily obtained.

ACKNOWLEDGEMENT

The author would like to acknowledge the assistance of Universal Energy Systems co-workers Max Lake, John Lawson, and Gerhard Mueller, and especially Rod Darrah. He would also like to thank Peter Bletzinger and Alan Garscadden of the Aeropropulsion Laboratory for their comments and suggestions.

References

1. Fellgett, P., "The Origins and Logic of Multiplex, Fourier, and Interferometric Methods in Spectrometry," Aspen Int. Conf. on Fourier Spectrosc., 1970 (Vanasse, G.A., Stair, Jr., A. T., and Baker, D.J., eds.) AFCRL-71-0019, 5 Jan. 1971, Spec. Rep. No. 114, p. 139.

2. Vanasse, G.A., and Sakai, H., "Fourier Spectroscopy", Progress in Optics, (E. Wolf, ed.), North Holand Publishing Co., Amsterdam, Vol. VI, p. 260, 1967.

3. Loewenstein, E. V., "Fourier Spectroscopy: An Introduction", Aspen Int. Conf. on Fourier Spectrosc. 1970 (Vanasse, G. A., Stair Jr., A. T., and Baker, D. J., eds.). AFCRL-71-0019, 5 Jan. 1971, Spec. Rep. No. 114, p. 3.

4. Bell, R. J., Introduction To Fourier Transform Spectroscopy, Academic Press, New York, 1972.

5. Born, M., and Wolf, E., Principles of Optics, Pergamor Press, 5th ed. 1975, chapter 10.

6. Titchmarsh, E. C., Introduction to the Theory of Fourier Integrals, Oxford At The Clarendon Press, 2nd ed. 1948.

7. Reference 5 uses complex analytic signals in the definitions of r_{11} and G(f), instead of the real rector potentials used here. The complex analytic signal is, however, directly related to the real vector potential (see ref. 5).

8. Lawson, J. L., and Uhlenbeck, G. E. Threshold Signals, M.I.T. Radiation Laboratory Series Vol. 34, McGraw-Hill Book Company Inc. 1950.

9. Sakai, H., "Considerations of the Signal-To-Noise Ratio in Fourier Spectroscopy", Aspen Int. Conf. on Fourier Spectroscopy 1970, (Vanasse, G. A., Stair, Jr., A. T., and Baker, D. J., eds.) AFCRL-71-0019, 5 Jan. 1971, Spec. Rep. No. 114, p. 19.

10. Gaydon, A. G., and Wolfhard, H. G., Flames, Their Structure, Radiation and Temperature, Chapman and Hall LTD, 3rd ed. 1970.

11. Herzberg, G., Infrared and Raman Spectra of Polyatomic Molecules, Van Nostrand Reinhold Company, 1945.

12. Ludwig, C. B., Malkmus, W., Reardon, J. E., and Thompson, J. A. L., Handbook of Infrared Radiation From Combustion Gases, (Goulard, R. and Thompson, J. A. L., eds.) NASA SP-3080, 1973.

13. Plyler, E. K., Blaine, L. R., and Tedwell, D., J. of Res. Nat. Bur. Std., Vol. 55, No. 4, p. 183, 1955.

14. Herzberg, G., Molecular Spectra and Molecular Structure I. - Spectra of Diatomic Molecules, Van Nostrand Reinhold Company, 2nd ed., 1950.

15. Merryman, E. L., and Levy, A., Fifteenth Symposium (International) on Combustion, p. 1073, 1974.

16. See Bevington, P. R., Data Reduction and Error Analysis for the Physical Sciences, chapter 11, McGraw - Hill Book Company, 1969.

17. Mantz, A. W., Maillard, J. - P., Roh, W. B., and Rao, K. N., J. Mol. Spec. 57, p. 155, 1975.

18. Heaps, H. S., and Herzberg, G., Zeit. Für Physik, 133, p. 48, (1952).